UNIVERSIDAD DE CONCEPCIÓN

Centro de Investigación en Ingeniería Matemática (CI^{2}MA)

Convergence analysis of a nonstandard finite volume method for a diffusion-production-destruction model

Abraham J. Arenas, Juan Barajas-Calonge,
Gilberto González-Parra, Luis M. Villada

PREPRINT 2026-22

SERIE DE PRE-PUBLICACIONES

CONVERGENCE ANALYSIS OF A NONSTANDARD FINITE VOLUME METHOD FOR A DIFFUSION-PRODUCTION-DESTRUCTION MODEL

ABRAHAM J. ARENAS[A], JUAN BARAJAS-CALONGE[B,*], GILBERTO GONZALEZ-PARRA[C], AND LUIS MIGUEL VILLADA[D]

Abstract. In this paper, we introduce and analyze a nonstandard finite volume (NSFV) scheme for a diffusion–production–destruction model. The numerical method is formulated by coupling an unconditionally stable nonstandard time discretization, which is dynamically consistent with the associated system of ordinary differential equations, with an implicit finite-volume discretization of the diffusion operator on triangular meshes. We establish the existence of a discrete solution to the NSFV scheme and, through non-negativity, L^2-estimates and compactness arguments, we prove the convergence of the scheme to an admissible weak solution of the model. We further develop a second-order extension in both space and time that preserves the positivity of the solutions. Finally, numerical experiments over two-dimensional spatial domains with complex geometries are presented to illustrate the behavior of the model and to assess the performance of the NSFV scheme.

1. Introduction

1.1. **Scope.** A wide variety of mathematical models for real-life problems are given in this form of partial differential equations (PDEs) of the diffusion-production-destruction type, in fields of science such as epidemiology [27, 53, 64], ecological modeling [65, 66], economics [52] and recently, in the field of artificial intelligence and data science [14,28,30,39,48], and a variety of works from different fields [1,26,44,55,62,67]. Because the underlying physical variables in these applications are inherently non-negative, the corresponding numerical schemes must satisfy these positivity constraints. In this paper, we propose and analyze a novel finite volume numerical scheme to solve a diffusion-production-destruction system of the form

$$\begin{aligned} &\frac{\partial u_i}{\partial t} = d_i \Delta u_i + f_i(\boldsymbol{u}) - u_i g_i(\boldsymbol{u}), \quad i = 1, \dots, N && \text{in } \Omega \times (0,T), \\ &\nabla u_i \cdot \boldsymbol{n} = 0, \quad i = 1, \dots, N && \text{on } \partial\Omega \times (0,T), \\ &u_i(\boldsymbol{x}, 0) = u_i^0(\boldsymbol{x}), \quad i = 1, \dots, N && \text{in } \Omega, \end{aligned} \tag{1.1}$$

where the unknown $\boldsymbol{u} = (u_1, \dots, u_N)^{\mathrm{T}}$ is a vector of physical quantities (such as chemical concentrations, densities or biological populations) that must remain non-negative, and $u_i = u_i(\boldsymbol{x}, t)$ are functions defined on $\Omega_T := \Omega \times (0,T)$, where $t > 0$ and $\Omega \subset \mathbb{R}^2$ is an open and bounded domain; $d_i > 0$ is the diffusion coefficient for the state variable i. Let $\mathbb{R}^N_+ = \{(x_1, \dots, x_N) \in \mathbb{R}^N : x_i \geq 0\}$, and let Σ be a prescribed subset

Date: July 7, 2026.

2010 *Mathematics Subject Classification.*

Key words and phrases.

*Corresponding author.

[A]Departamento de Matemáticas y Estadística, Universidad de Córdoba, Carrera 6 No. 77 - 305, Montería, Colombia and Department of Mathematics, New Mexico Tech, 801 Leroy Pl, Socorro, USA. E-Mail: aarenas@correo.unicordoba.edu.co.

[B]GIMNAP-Departamento de Matemática, Universidad del Bío-Bío, Casilla 5-C, Concepción, Chile and Departamento de Ciencias Naturales y Tecnología, Universidad de Aysén, Lillo 667, Coyhaique, Chile. E-Mail: juan.barajas2001@alumnos.ubiobio.cl.

[C] Department of Mathematics, New Mexico Tech, 801 Leroy Pl, Socorro, 87801, USA. E-Mail: gilberto.gonzalezparra@nmt.edu.

[D]GIMNAP-Departamento de Matemáticas, Universidad del Bío-Bío, Casilla 5-C, Concepción, Chile, and CI^{2}MA, Universidad de Concepción, Casilla 160-C, Concepción, Chile. E-Mail: lvillada@ubiobio.cl.

of $\mathbb{R}^N_+$. The functions $f_i, g_i : \Sigma \subseteq \mathbb{R}^N_+ \longrightarrow \mathbb{R}$ are functional responses satisfying the following assumptions:

$$\begin{aligned} &f_i, g_i \in \mathcal{C}^2(\Sigma;\mathbb{R}), \quad f_i(\boldsymbol{u}),\, g_i(\boldsymbol{u}) \geq 0, \\ &|f_i(\boldsymbol{u})| \leq K_f\,(1+\|\boldsymbol{u}\|_1)\,,\, |g_i(\boldsymbol{u})| \leq K_g, \end{aligned} \qquad \forall\, \boldsymbol{u} \in \Sigma \subseteq \mathbb{R}^N_+, \quad i = 1,\ldots,N, \tag{1.2}$$

In addition, we are interested in ensuring that the numerical scheme guarantees dynamical consistency with respect to the model $\boldsymbol{u}_t = \boldsymbol{F}(\boldsymbol{u})$, which is the spatially homogeneous version of (1.1). In this regard, the non-standard finite difference (NSFD) method, first developed by Mickens [41], provides design rules for approximating ODE systems using unconditionally stable schemes that preserve key qualitative characteristics of the original continuous system, such as positivity, boundedness, and asymptotic behavior [20,45,47]. Now, with respect to PDE problems, these NSFD schemes are usually combined with finite difference methods (FDM) and finite volume methods (FVM) to approximate solutions in a wide range of applications such as epidemiology [3,10,16,33,42,63], biological populations [18,46,49,54] and other applications [2,8,23,33,47], where numerical schemes have been proposed and properties such as positivity and boundedness have been studied, however, an analysis of the numerical convergence scheme to a solution of PDE is not performed. Furthermore, on the one hand, the use of finite differences to approximate spatial derivatives limits the applications to rectangular domains. On the other hand, FVM is a widely used spatial discretization technique for numerical simulations across various engineering fields, including fluid mechanics, heat and mass transfer, and petroleum engineering, among others. It can be applied to arbitrary geometries using either structured or unstructured meshes, and it offers robust schemes whose convergence to the weak solution of the PDE can be rigorously analyzed [24].

This paper has a twofold objective. The first objective is to introduce an unconditionally stable numerical scheme for approximating the solution of (1.1). This approach combines an implicit finite-volume discretization on general triangular meshes with a nonstandard treatment of the reaction terms. In addition, we provide a comprehensive numerical analysis establishing convergence toward a weak solution of (1.1), thereby yielding a reliable computational tool for applications in general two-dimensional spatial domains with complex geometries. The second objective is to extend the proposed numerical scheme to achieve second-order accuracy in both space and time, while preserving the positivity property of the first-order method.

1.2. **Related work.** Mathematical models based on PDEs have been growing in recent years [21,29,35,51, 56]. With regard to advection-diffusion-production-destruction systems, in [43] a numerical method based on the method of lines and Runge-Kutta was developed. In [36] a comparison of modified Patankar-Runge-Kutta schemes and standard ODE solvers for an advection-diffusion-production system was presented to show the positivity of the solutions by the former schemes. Recently, in [17] a mathematical model of infectious disease with a chemotaxis-type term was proposed. Numerical simulations of the model were shown in which the propagation of a disease was shown over long spatial distances.

NSFD methods have been developed to approach the solution of various applications described by PDEs. In ecology, in [18], an NSFD scheme was proposed to solve a reaction-diffusion model describing the coexistence of plant species in arid environments, in [45] a theta NSFD scheme was developed for a Lotka-Volterra model. In epidemiology, in [42], an NSFD scheme was analyzed for a system of partial differential equations representing a spatial SIR epidemic model. The well-known Black–Scholes equation is fundamentally a diffusion-type PDE that has been numerically solved using NSFD schemes [8, 23]. With regard to the advection-diffusion-reaction equation, NSFD schemes were developed and studied in [6, 49, 54]. In addition, the NSFD methodology has been applied to Sobolev type PDEs [40]. In [47] a complete review of different applications of NSFD schemes is provided.

With regard to the finite volume method in [46] an explicit characteristic-based finite volume method was developed to numerically solve some advection-diffusion-reaction equations. In [10], NSFD and finite volume schemes were designed to solve a Holling-Tanner predator-prey model. In addition, in [50] a modification of Wang's finite volume method was used to solve the Black-Scholes equation. In [2] a NSFV method was developed to numerically solve the Schrödinger equation, where the perturbation term is approximated by the nonstandard technique and the potential is approximated by its mean value in the cell. In [4] the

authors developed a semi-implicit finite volume method to numerically solve a mathematical model of biofilm formation in a non-orthogonal grid system. In [7] several finite volume methods were designed to solve the 2D convective Cahn–Hilliard equation and the nonlinear terms were approximated using NSFD foundations. In [59] nonstandard multistep methods were studied and it was found that under some conditions these methods have the same order as the classical multistep methods. Moreover, the preservation of some qualitative properties for any step size was proven.
With regard to higher order methods, several researchers have worked with models based on PDEs and especially with reaction-diffusion terms or similar [60,63]. In [63] a higher-order NSFD scheme was developed and modified using Richardson's extrapolation. In [16] a time discretization scheme was developed for a model of co–infection dynamics in a heterogeneous population. Thus, based on the aforementioned work in the topics of advection-diffusion-production-destruction systems, NSFD schemes, finite volume method and higher order methods, we can see that is an active field of research.
Our main contribution in this work is the combination of non-standard schemes, finite volume and higher order methodologies in a single work to numerically solve a general diffusion-production-destruction model. Specifically, we propose an NSFV scheme and, through a rigorous proof, demonstrate its convergence to a weak admissible solution of the model; this scheme preserves the positivity of the solutions, among other mathematical properties. Furthermore, we extend our work to a second-order NSFV scheme via a Strang operator splitting. Thus, we will establish a second-order NSFD integrator for a reaction subsystem combined with a finite volume spatial discretization.

1.3. **Outline of the paper.** The remainder of the paper is organized as follows. Section 2 provides the description of the FV method employed. In Section 2.1 we develop the first order NSFD scheme and show that it preserves dynamical properties such as positivity and equilibrium points of the spatially-homogeneous version of (1.1). In Section 2.3, we present the FV discretization of equations (1.1), where we approximate the reaction term by the described NSFD approach, first recalling in Section 2.2 the standard admissible-mesh notation from [24]. Section 3 focuses on establishing the convergence of the NSFV scheme as the mesh size tends to zero. Since the method is implicit and requires solving linear algebraic systems at each time level, we must first establish that the scheme is well defined and admits a solution at each step. This is addressed in Section 3.1 in Theorem 3.2, where we also check that the discrete solution generated by the NSFV scheme remains non-negative. In Section 3.2 we show an a priori L^2 estimate for the discrete solutions required to prove the convergence of the scheme. In Section 3.3 we establish compactness results for the family of discrete solutions, and in Section 3.4 we verify that any limit point of these solutions is an admissible weak solution of (1.1). In Section 4 we construct a positivity-preserving scheme, and that is also second order in both space and time. In Section 5, we present some numerical examples. Examples 1 and 2 illustrate the convergence and robustness of the NSFD-2 discretization, while Example 3 examines the convergence in both space and time of the studied NSFV, NSFV-1, and NSFV-2 numerical methods. Finally, in Example 4 we apply the convergent NSFV scheme to a variety of settings, simulating the behavior of models on two-dimensional domains with complex geometries.

2. NSFV for reaction-diffusion model

In this section, we propose a finite volume scheme for approximating the model (1.1). We first describe the NSFD discretization of the spatially homogeneous model, which we then combine with a traditional two-point flux approximation for the spatial operators.

2.1. **NSFD for the spatially homogeneous model.** To describe the NSFD discretization approach, let us consider a general Cauchy problem of the form

$$\begin{aligned} \frac{d\boldsymbol{z}}{dt} &= \boldsymbol{f}(\boldsymbol{z}), \text{ in } [0,T] \\ \boldsymbol{z}(t_0) &= \boldsymbol{z}_0, \end{aligned} \tag{2.1}$$

where T is a positive real number, $\boldsymbol{z} = (z_1, z_2, \ldots, z_N)^{\mathrm{T}} : [0,T] \to \mathbb{R}^N$, and the function $\boldsymbol{f} = (f_1, f_2, \ldots, f_N)^{\mathrm{T}} : \mathbb{R}^N \to \mathbb{R}^N$ is differentiable at $\boldsymbol{z}_0 \in \mathbb{R}^N$. First, we discretize the computational domain $[0,T]$ by partitioning

$t^n = n\Delta t$, where $\Delta t = T/M$ is the step size and M is a fixed positive integer. A numerical scheme with step size Δt that approximates the solution $\boldsymbol{z}(t^n)$ of the system (2.1) can be written as

$$\boldsymbol{\mathcal{D}}_{\Delta t}(\boldsymbol{z}^n) = \boldsymbol{F}_{\Delta t}(\boldsymbol{f}; \boldsymbol{z}^n), \tag{2.2}$$

where, $\boldsymbol{\mathcal{D}}_{\Delta t}(\boldsymbol{z}^n) \approx \left.\frac{d\boldsymbol{z}}{dt}\right|_{t=t^n}$, $\boldsymbol{z}^n \approx \boldsymbol{z}(t^n)$, and $\boldsymbol{F}_{\Delta t}(\boldsymbol{f}; \boldsymbol{z}^n)$ approximate the right side of the system (2.1).

Definition 2.1. *The numerical scheme given by (2.2) is called a Nonstandard Finite Difference (NSFD) scheme if at least one of the following conditions is satisfied,*

(1) $\boldsymbol{\mathcal{D}}_{\Delta t}(\boldsymbol{z}^n) = \dfrac{\boldsymbol{z}^{n+1} - \boldsymbol{z}^n}{\varphi(\Delta t)}$*, where* φ *is a non-negative real valued function that satisfies*

$$\varphi(\Delta t) = \Delta t + \mathcal{O}(\Delta t^2).$$

(2) $\boldsymbol{F}_{\Delta t}(\boldsymbol{f}; \boldsymbol{z}^n) = \boldsymbol{G}(\boldsymbol{z}^n, \boldsymbol{z}^{n+1}, \Delta t)$*, where* $\boldsymbol{G}(\boldsymbol{z}_n, \boldsymbol{z}^{n+1}, \Delta t)$ *is a non-local approximation of the right side of the system (2.1).*

Some examples of denominator functions satisfying condition (1) in the above definition are:

$$\varphi(\Delta t) = \frac{1 - e^{-\lambda \Delta t}}{\lambda},\ \lambda > 0,\ \varphi(\Delta t) = e^{\Delta t} - 1, \text{see [41]}. \tag{2.3}$$

Now, using Definition 2.1 we design a numerical scheme to numerically approximate the solutions of spatially homogeneous system $\boldsymbol{u}_t = \boldsymbol{F}(\boldsymbol{u})$. Let $i \in \{1, \ldots, N\}$ be given. We denote by u_i^n the approximation $u_i(t^n)$ for $n = 0, 1, 2...$ and by $\boldsymbol{F} = (F_1, \ldots, F_N)^{\mathrm{T}}$ the right-hand side function in (1.1). To facilitate notation, we set $\boldsymbol{u}^n = (u_1^n, \ldots, u_N^n)$ and omit the dependence of these variables whenever the context is clear. We proceed as follows:

(1) Implement the non-local approximations on the right-hand side of (1.1):

$$F_i(\boldsymbol{u}) \approx f_i(\boldsymbol{u}^n) - g_i(\boldsymbol{u}^n) u_i^{n+1}, \quad i = 1, \ldots, N. \tag{2.4}$$

(2) The first-order derivatives of the system (1.1) are approximated by:

$$\frac{du_i}{dt} \approx \frac{u_i^{n+1} - u_i^n}{\varphi_i(\Delta t)}, \quad i = 1, \ldots, N, \tag{2.5}$$

where the denominator functions φ_i for $i = 1, \ldots, N$ satisfy (1) in Definition 2.1.

Hence, the system (1.1) can be discretized as

$$\frac{u_i^{n+1} - u_i^n}{\varphi_i(\Delta t)} = f_i(\boldsymbol{u}^n) - g_i(\boldsymbol{u}^n) u_i^{n+1}, \quad i = 1, \ldots, N. \tag{2.6}$$

If we rewrite the system in an explicit form, we obtain

$$u_i^{n+1} = \frac{u_i^n + \varphi_i(\Delta t) f_i(\boldsymbol{u}^n)}{1 + \varphi_i(\Delta t) g_i(\boldsymbol{u}^n)}, \quad i = 1, \ldots, N. \tag{2.7}$$

which clearly produces non-negative solutions. We also notice that we can rewrite the system (2.7) as

$$u_i^{n+1} = u_i^n + F_i(\boldsymbol{u}^n) G_i(\Delta t, \boldsymbol{u}^n), \quad G_i(\Delta t, \boldsymbol{u}^n) := \frac{\varphi_i(\Delta t)}{1 + \varphi_i(\Delta t) g_i(\boldsymbol{u}^n)}, \quad i = 1, \ldots, N. \tag{2.8}$$

Let us find the equilibrium points of the scheme (2.7). To this end, we have to solve the system $\boldsymbol{u}^{n+1} = \boldsymbol{u}^n$, i.e $u_i^{n+1} = u_i^n$, for all $i = 1, \ldots, N$. By using (2.8) we get that $F_i(\boldsymbol{u}^n) G_i(\Delta t, \boldsymbol{u}^n) = 0$. Being G_i positive functions, it follows that $F_i(\boldsymbol{u}^n) = 0$, for $i = 1, \ldots, N$. Therefore, the system (2.7) and the continuous-time model $\boldsymbol{u}_t = \boldsymbol{F}(\boldsymbol{u})$ have the same sets of equilibria.

We refer to the scheme (2.7) as NSFD-1 method. Now, we aim to discretize the diffusion-reaction model (1.1) using a technique that preserves these important biological properties of the associated ODE system. To do so, we explore a combination of the standard Finite Volume Method in general grids. To this end, we introduce the notion of an admissible finite volume mesh (cf. [24]).

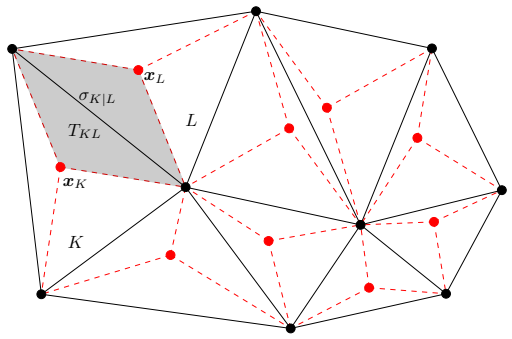

FIGURE 2.1. Control volumes, centers and diamonds (in dashed lines).

2.2. **Space and time discretization meshes.** Let us begin by describing the discretization of the spatial domain. For this purpose, we assume that the domain $\Omega \subset \mathbb{R}^2$ is polygonal.

Definition 2.2. *An admissible mesh for Ω can be defined as a triplet $(\mathcal{T}, \mathcal{E}, \mathcal{P})$, where $\mathcal{T}$ is a finite collection of non-overlapping, bounded, convex polygonal subsets of Ω called control volumes, $\mathcal{E}$ is a finite collection of subsets of $\overline{\Omega}$, each contained in a hyperplane of $\mathbb{R}^2$, having strictly positive one-dimensional measure and referred to as the edges of the control volumes, and $\mathcal{P} = (\boldsymbol{x}_K)_{K\in\mathcal{T}}$ is a finite collection of points in Ω, known as the centers of the control volumes. This definition is employed to describe the discretization of the domain within the framework of the finite volume method. The triplet $(\mathcal{T}, \mathcal{E}, \mathcal{P})$ has the following properties:*

(1) The union of the closures of all control volumes is $\overline{\Omega}$, i.e. $\overline{\Omega} = \bigcup_{K\in\mathcal{T}} \overline{K}$.
(2) For any $K \in \mathcal{T}$, there exists $\mathcal{E}_K \subset \mathcal{E}$ such that $\partial K = \overline{K} - K = \bigcup_{\sigma\mathcal{E}_K} \overline{\sigma}$. Moreover, $\mathcal{E} = \bigcup_{K\in\mathcal{T}} \mathcal{E}_K$.
(3) For any $(K, L) \in \mathcal{T}^2$ with $K \neq L$, either the length of $\overline{K} \cap \overline{L}$ is 0 or $\overline{K} \cap \overline{L} = \overline{\sigma}$, for some $\sigma \in \mathcal{E}$, which will be denoted by $\sigma_{K|L}$.
(4) The family $\mathcal{P} = (\boldsymbol{x}_K)_{K\in\mathcal{T}}$ is such that $\boldsymbol{x}_K \in \overline{K}$, for all $K \in \mathcal{T}$. In addition, if $\sigma = \sigma_{K|L}$, we assume that $\boldsymbol{x}_K \neq \boldsymbol{x}_L$ and the straight line $\mathcal{D}_{K,L}$ going through $\boldsymbol{x}_K$ and $\boldsymbol{x}_L$ is orthogonal to $K|L$.
(5) For any $\sigma \in \mathcal{E}$ with $\sigma \subset \partial\Omega$, denote by K the control volume such that $\sigma \in \mathcal{E}_K$. If $\boldsymbol{x}_K \notin \sigma$, let $\mathcal{D}_{K,\sigma}$ denote the line through $\boldsymbol{x}_K$ orthogonal to σ. We assume $\mathcal{D}_{K,\sigma} \neq \emptyset$ and define $\boldsymbol{y}_\sigma = \mathcal{D}_{K,\sigma} \cap \sigma$.

We introduce the following notations. The size of the mesh $\mathcal{T}$ is defined by

$$\operatorname{size}(\mathcal{T}) = \max_{K\in\mathcal{T}} \operatorname{diam}(K),$$

where $\operatorname{diam}(K) = \max_{\boldsymbol{x},\boldsymbol{y}\in K} \|\boldsymbol{x} - \boldsymbol{y}\|_2$. We denote by $\mathcal{N}(K)$ the set of neighbors of the control volume K, i.e., $\mathcal{N}(K) = \{L \in \mathcal{T} : \overline{K} \cap \overline{L} = \overline{\sigma}, \text{ for some } \sigma \in \mathcal{E}\}$; a generic neighbor of K is denoted by L. Moreover, we denote by $\boldsymbol{n}_{K|L}$ and $d_{K|L}$ the unit normal vector to $\sigma_{K|L}$ outward from K and the distance $\|\boldsymbol{x}_K - \boldsymbol{x}_L\|_2$, respectively. For any $K \in \mathcal{T}$ and $\sigma \in \mathcal{E}$, we denote by $m(K)$ the 2−dimensional Lebesgue measure of K. If $L \in \mathcal{N}(K)$, then $m(\sigma_{K|L})$ will denote the 1−dimensional measure of the edge $\sigma_{K|L}$, and finally, the transmissibility through $\sigma_{K|L}$ is defined as $\tau_{K|L} := \frac{m(\sigma_{K|L})}{d_{K|L}}$. The discrete unknowns are piecewise constant functions on the control volumes $K \in \mathcal{T}$, so we introduce the Hilbert space

$$H_{\mathcal{T}}(\Omega) = \left\{\phi \in L^2(\Omega) : \phi|_K \in \mathbb{P}_0(K), \quad \forall K \in \mathcal{T}\right\}. \tag{2.9}$$

Thus, every function $u_{\mathcal{T}} \in H_{\mathcal{T}}(\Omega)$ is characterized by its numerical values $(u_K)_{K\in\mathcal{T}}$ such that $u_{\mathcal{T}}|_K = u_K$ for every $K \in \mathcal{T}$. It is clear that $H_{\mathcal{T}}(\Omega) \subset L^2(\Omega)$ and the usual inner scalar product and norm become

$$\left(u_{\mathcal{T}}, v_{\mathcal{T}}\right)_{0,\Omega} = \sum_{K\in\mathcal{T}} m(K) u_K v_K, \quad \|u_{\mathcal{T}}\|_{0,\Omega} = \left(\sum_{K\in\mathcal{T}} m(K)|u_K|^2\right)^{1/2}, \quad \forall\, u_{\mathcal{T}}, v_{\mathcal{T}} \in H_{\mathcal{T}}(\Omega).$$

We also introduce the discrete semi-norm

$$|u_{\mathcal{T}}|_{1,\mathcal{T}}^2 := \frac{1}{2}\sum_{K\in\mathcal{T}}\sum_{L\in\mathcal{N}(K)}\tau_{K|L}|u_L-u_K|^2, \quad \forall\, u_{\mathcal{T}}\in H_{\mathcal{T}}(\Omega). \tag{2.10}$$

Moreover, for an interface $\sigma_{K|L}\in\mathcal{E}$ of a control volume K, we consider the "diamond" T_{KL} constructed by joining the diamond centers $\boldsymbol{x}_K$ and $\boldsymbol{x}_L$ with the extremes of the interval (see Figure 2.1). The discrete gradient operator $\nabla_{\mathcal{T}}$ of a function $u_{\mathcal{T}}\in H_{\mathcal{T}}(\Omega)$ is a piecewise constant function over the diamonds T_{KL} such that

$$\nabla_{\mathcal{T}}u_{\mathcal{T}}|_{T_{KL}} := \begin{cases} 2\dfrac{u_L-u_K}{d_{K|L}}\boldsymbol{n}_{K|L}, & \text{for } \sigma=\sigma_{K|L}\in\mathcal{E}\setminus\partial\Omega,\\ 0, & \text{for } \sigma\in\partial K. \end{cases} \tag{2.11}$$

We define the size of the space–time discretization by $h := \max(\mathrm{size}(\mathcal{T}),\Delta t)$. Finally, the complete discrete solution is a time-sequence of piecewise constant functions $(u_{\mathcal{T}}^n)_{n\in\mathbb{N}}$ such that $u_{\mathcal{T}}^n\in H_{\mathcal{T}}(\Omega)$, for all n. In addition, we associate a time and space piecewise constant function with this sequence denoted by u_h and defined by

$$u_h(\boldsymbol{x},t) = u_K^{n+1}, \quad \text{for a.e.} \quad (\boldsymbol{x},t)\in K\times(t_n,t_{n+1}), \quad \forall K\in\mathcal{T},\,\forall n\in\{0,1,\dots,N\}. \tag{2.12}$$

2.3. **The finite volume nonstandard scheme.** The Finite Volume scheme for (1.1) is stated as follows: for all $K\in\mathcal{T}$ and $n\in\{0,1,\dots,M\}$, find $\{u_{i,K}^{n+1}\}_{K\in\mathcal{T}}$ such that

$$m(K)\frac{u_{i,K}^{n+1}-u_{i,K}^n}{\Delta t} - d_i\sum_{L\in\mathcal{N}(K)}\tau_{K|L}(u_{i,L}^{n+1}-u_{i,K}^{n+1}) = m(K)\bar{F}_i(\boldsymbol{u}_K^n,\boldsymbol{u}_K^{n+1}), \quad i=1,\dots,N, \tag{2.13}$$

where the right-hand side functions are approximated by a semi-implicit approach in the sense that the right-hand side contributions depend on the numerical solution at times $t=t_n$ and $t=t_{n+1}$, i.e., we define:

$$\bar{F}_i(\boldsymbol{u}_K^n,\boldsymbol{u}_K^{n+1}) = f_i(\boldsymbol{u}_K^n) - g_i(\boldsymbol{u}_K^n)u_{i,K}^{n+1}, \quad i=1,\dots,N., \tag{2.14}$$

This discretization is selected to ensure the dynamic consistency of the scheme and coincides with the NSFD approximation described in Section 2.1, with $\varphi_i(\Delta t)=\Delta t$, for $i=1,\dots,N$.
As usual, homogeneous Neumann boundary conditions are incorporated implicitly. Specifically, the portions of ∂K that lie in $\partial\Omega$ do not contribute to the sums over $L\in\mathcal{N}(K)$ terms, which effectively enforces a zero–flux condition along the outer edges of the mesh.

3. Convergence of the NSFV scheme

In this section, we establish the well-posedness of the discrete system and derive a priori estimates needed to prove the convergence of the NSFV method (2.13) toward a weak solution of system (1.1). To this end, we first introduce the notion of a weak solution.

Definition 3.1. *Given functions $\boldsymbol{u}^0=(u_1^0,\dots,u_N^0)^{\mathrm{T}}$ defined a.e. in Ω such that $\boldsymbol{u}^0\in\mathbb{R}_+^N$ a.e. in Ω, we define a weak solution of (1.1) as a set of functions $\boldsymbol{u}=(u_1,\dots,u_N)^{\mathrm{T}}$ defined a.e. in $\Omega_T:=\Omega\times(0,T)$, such that $\boldsymbol{u}\in\mathbb{R}_+^N$ a.e. in Ω_T, $\boldsymbol{u}_i\in L^2(0,T;H^1(\Omega))$, $i=1,\dots,N$ and for any test functions $\psi_i\in\mathcal{D}(\overline{\Omega}\times[0,T))$, $i=1,\dots,N$ the function $\boldsymbol{u}$ satisfies the following identities:*

$$\begin{aligned} -\iint_{\Omega_T} u_i\partial_t\psi_i\,\mathrm{d}\boldsymbol{x}\,\mathrm{d}t + \iint_{\Omega_T} d_i\nabla u_i\cdot\nabla\psi_i\,\mathrm{d}\boldsymbol{x}\,\mathrm{d}t \\ = \iint_{\Omega_T} F_i(\boldsymbol{u})\cdot\psi_i\,\mathrm{d}\boldsymbol{x}\,\mathrm{d}t + \int_\Omega u_i^0(\boldsymbol{x})\psi_i(\boldsymbol{x},0)\,\mathrm{d}\boldsymbol{x}, \end{aligned} \qquad i=1,\dots,N. \tag{3.1}$$

3.1. **Well-posedness of the discrete system.** Let us proceed to prove the well-posedness of discrete system (2.13).

Theorem 3.2. *Let $\mathcal{T}$ be an admissible discretization of Ω and $\boldsymbol{u}^0 \in \mathbb{R}_+^N$. Then, the discrete problem* (2.13) *has a unique solution $(\boldsymbol{u}_K^{n+1})_{K\in\mathcal{T},n\in\{0,\dots,M\}}$ such that $\boldsymbol{u}_K^{n+1} \in \mathbb{R}_+^N$, for all $K \in \mathcal{T}$, $n \in \{0,\dots,M\}$.*

Proof. Given an admissible mesh $\mathcal{T}$, let us denote by N_e the number of control volumes of $\mathcal{T}$ and by $\mathbf{u}_i^n \in \mathbb{R}^{N_e}$, $i = 1,\dots,N$, the vectors of unknowns at time $t = t^n$. To state the algorithm, we define the following vectors of $\mathbb{R}^{N_e}$ which are evaluated at time $t = t^n$:

$$\mathbf{f}_i^n := \big(f_i(\boldsymbol{u}_K^n)\big)_{K=1}^{N_e},\ \mathbf{g}_i^n := \big(g_i(\boldsymbol{u}_K^n)\big)_{K=1}^{N_e},\quad i = 1,\dots,N.$$

We also introduce the Hadamard product $\mathbf{u} * \mathbf{v}$, which is defined for vectors $\mathbf{u},\mathbf{v} \in \mathbb{R}^{N_e}$ as $(\mathbf{u}*\mathbf{v})_j = u_j v_j$, for $j = 1,\dots,N_e$, we denote by $\mathrm{diag}(\mathbf{v})$ the diagonal matrix with the vector $\mathbf{v} \in \mathbb{R}^{N_e}$ in the diagonal, by $\mathbf{I} \in \mathbb{R}^{N_e\times N_e}$ the identity matrix of size $N_e \times N_e$, and by $\mathbf{1} \in \mathbb{R}^{N_e}$ a vector of ones of size N_e. Let $\mathcal{L} \in \mathbb{R}^{N_e\times N_e}$ be the discretization of the Laplacian operator defined by

$$(\mathcal{L})_{KL} := \begin{cases} -\dfrac{1}{m(K)} \displaystyle\sum_{L'\in\mathcal{N}(K)} \tau_{K|L'}, & L = K, \\ \dfrac{\tau_{K|L}}{m(K)}, & L \in \mathcal{N}(K), \\ 0, & \text{otherwise}, \end{cases} \tag{3.2}$$

Within this notation, equation (2.13) becomes

$$\frac{u_{i,K}^{n+1} - u_{i,K}^n}{\Delta t} - d_i(\mathcal{L}\mathbf{u}_i^{n+1})_K = f_i(\boldsymbol{u}_K^n) - g_i(\boldsymbol{u}_K^n)u_{i,K}^{n+1},\quad i = 1,\dots,N$$

which is linear in $\mathbf{u}_i^{n+1}$. Then, by rearranging the terms in vector form, we obtain

$$[\mathbf{I} - \Delta t d_i\mathcal{L} + \Delta t\mathrm{diag}(\mathbf{g}_i^n)]\mathbf{u}_i^{n+1} = \mathbf{u}_i^n + \Delta t\mathbf{f}_i^n,\quad i = 1,\dots,N. \tag{3.3}$$

Notice that the matrix $\mathbb{M}_i = \mathbf{I} - \Delta t d_i\mathcal{L} + \Delta t\mathrm{diag}(\mathbf{g}_i^n)$ has the entry structure

$$(\mathbb{M}_i)_{KL} = \begin{cases} 1 + \Delta t d_i \displaystyle\sum_{L'\in\mathcal{N}(K)} \frac{\tau_{K|L'}}{m(K)} > 0, & L = K, \\ -\Delta t\, d_i\, \dfrac{\tau_{K|L}}{m(K)} \le 0, & L \in \mathcal{N}(K). \end{cases} \tag{3.4}$$

and thus is strictly diagonally dominant by rows, since

$$(\mathbb{M}_i)_{KK} = 1 + \Delta t\, d_i \sum_{L\in\mathcal{N}(K)} \frac{\tau_{K|L}}{m(K)} > \sum_{L\in\mathcal{N}(K)} |(\mathbb{M}_i)_{KL}|, \tag{3.5}$$

In this way we see that $\mathbb{M}_i$ is a non-singular M-matrix and therefore has a nonnegative inverse [13, Theorem 6.2.3]. Thus, the system (3.3) has a unique solution, and $\mathbf{u}_i^{n+1} = \mathbb{M}_i^{-1}(\mathbf{u}_i^n + \Delta t\mathbf{f}_i^n) \ge 0$. □

3.2. **Discrete estimates.** In this section, following arguments analogous to those in [5,19,24], we establish the discrete estimates required to prove the convergence of scheme (2.13) towards a weak solution of (1.1).

Lemma 3.3. *Let $(\boldsymbol{u}_K^{n+1})_{K\in\mathcal{T},n\in\{0,\dots,M\}}$ be a solution of* (2.13)*. Then there are constants $C^*, C_* > 0$ depending on the L^2-norm of the initial condition $\|\boldsymbol{u}^0\|_{0,\Omega}$ and the parameters of the model, such that*

$$\sum_{i=1}^N \left(\max_{n\in\{0,1,\dots,M\}} \sum_{K\in\mathcal{T}} m(K)(u_{i,K}^{n+1})^2 \right) \le C_*, \tag{3.6}$$

$$\frac{1}{2}\sum_{i=1}^N \sum_{n=0}^M \Delta t \sum_{K\in\mathcal{T}} \sum_{L\in\mathcal{N}(K)} \tau_{K|L}(u_{i,L}^{n+1} - u_{i,K}^{n+1})^2 \le C^*. \tag{3.7}$$

Proof. We start the proof by multiplying (2.13) by $\Delta t u_{i,K}^{n+1}$ and adding the result over $i \in \{1,\dots,N\}, K \in \mathcal{T}$, and $n \in \{0,\dots,M\}$ to obtain the identity $X_1 + X_2 + X_3 = 0$, where

$$
\begin{aligned}
X_1 &:= \sum_{i=1}^{N}\sum_{n=0}^{M}\sum_{K\in\mathcal{T}} m(K)(u_{i,K}^{n+1} - u_{i,K}^{n})u_{i,K}^{n+1},\\
X_2 &:= -\sum_{i=1}^{N} d_i \sum_{n=0}^{M}\Delta t \sum_{K\in\mathcal{T}}\sum_{L\in\mathcal{N}(K)} \tau_{K|L}(u_{i,L}^{n+1} - u_{i,K}^{n+1})u_{i,K}^{n+1},\\
X_3 &:= -\sum_{i=1}^{N}\sum_{n=0}^{M}\Delta t \sum_{K\in\mathcal{T}} m(K)\bar{F}_i(\boldsymbol{u}_K^n, \boldsymbol{u}_K^{n+1})u_{i,K}^{n+1}.
\end{aligned}
$$

Using the inequality "$a(a-b) \geq \frac{1}{2}(a^2 - b^2)$ for $a, b \in \mathbb{R}$" we get a lower bound for X_1 given by:

$$
X_1 \geq \frac{1}{2}\sum_{i=1}^{N}\sum_{n=0}^{M}\sum_{K\in\mathcal{T}} m(K)\Big((u_{i,K}^{n+1})^2 - (u_{i,K}^{n})^2\Big) = \frac{1}{2}\sum_{i=1}^{N}\sum_{K\in\mathcal{T}} m(K)\Big((u_{i,K}^{M+1})^2 - (u_{i,K}^{0})^2\Big).
$$

Now, by using the identity $2a(a-b) = a^2 - b^2 + (a-b)^2$ and gathering the edges, we can write

$$
\begin{aligned}
X_2 &= \frac{1}{2}\sum_{i=1}^{N} d_i \sum_{n=0}^{M}\Delta t \sum_{K\in\mathcal{T}}\sum_{L\in\mathcal{N}(K)} \tau_{K|L}\Big((u_{i,L}^{n+1})^2 - (u_{i,K}^{n+1})^2 + (u_{i,L}^{n+1} - u_{i,K}^{n+1})^2\Big)\\
&= \frac{1}{2}\sum_{i=1}^{N} d_i \sum_{n=0}^{M}\Delta t \sum_{K\in\mathcal{T}}\sum_{L\in\mathcal{N}(K)} \tau_{K|L}(u_{i,L}^{n+1} - u_{i,K}^{n+1})^2\\
&\quad + \frac{1}{2}\sum_{i=1}^{N} d_i \sum_{n=0}^{M}\Delta t \sum_{K\in\mathcal{T}}\sum_{L\in\mathcal{N}(K)} \tau_{K|L}\big[(u_{i,L}^{n+1})^2 - (u_{i,K}^{n+1})^2\big]\\
&= \frac{1}{2}\sum_{i=1}^{N} d_i \sum_{n=0}^{M}\Delta t \sum_{K\in\mathcal{T}}\sum_{L\in\mathcal{N}(K)} \tau_{K|L}(u_{i,L}^{n+1} - u_{i,K}^{n+1})^2.
\end{aligned}
$$

Finally, from Assumptions (1.2), Theorem 3.2, and Young's inequality, we get

$$
\begin{aligned}
X_3 =& -\sum_{i=1}^{N}\sum_{n=0}^{M}\Delta t \sum_{K\in\mathcal{T}} m(K)\bar{F}_i(\boldsymbol{u}_K^n, \boldsymbol{u}_K^{n+1})u_{i,K}^{n+1}\\
=& \sum_{i=1}^{N}\sum_{n=0}^{M}\Delta t \sum_{K\in\mathcal{T}} m(K) g_i(\boldsymbol{u}_K^n)(u_{i,K}^{n+1})^2 - \sum_{i=1}^{N}\sum_{n=0}^{M}\Delta t \sum_{K\in\mathcal{T}} m(K) f_i(\boldsymbol{u}_K^n)u_{i,K}^{n+1}\\
\geq& -K_f \sum_{i=1}^{N}\sum_{n=0}^{M}\Delta t \sum_{K\in\mathcal{T}} m(K) - K_f \sum_{i=1}^{N}\sum_{j=1}^{N}\sum_{n=0}^{M}\Delta t \sum_{K\in\mathcal{T}} m(K)|u_{j,K}^{n}||u_{i,K}^{n+1}|\\
\geq& -K_f m(\Omega)NT - \frac{K_f N}{2}\sum_{i=1}^{N}\sum_{n=0}^{M}\Delta t \sum_{K\in\mathcal{T}} m(K)(u_{i,K}^{n})^2 - \frac{K_f N}{2}\sum_{i=1}^{N}\sum_{n=0}^{M}\Delta t \sum_{K\in\mathcal{T}} m(K)(u_{i,K}^{n+1})^2\\
=& -C_1 - C_2\sum_{i=1}^{N}\Delta t \sum_{K\in\mathcal{T}} m(K)(u_{i,K}^{0})^2 - C_3\sum_{i=1}^{N}\sum_{n=0}^{M}\Delta t \sum_{K\in\mathcal{T}} m(K)(u_{i,K}^{n+1})^2\\
\geq& -C_1 - C_2 M\Delta t\|\boldsymbol{u}^0\|_{0,\Omega}^2 - C_3\sum_{i=1}^{N}\sum_{n=0}^{M}\Delta t \sum_{K\in\mathcal{T}} m(K)(u_{i,K}^{n+1})^2
\end{aligned}
$$

$$:= - C_4 - C_3 \sum_{i=1}^{N} \sum_{n=0}^{M} \Delta t \sum_{K\in\mathcal{T}} m(K)(u_{i,K}^{n+1})^2,$$

where $C_1, C_2, C_3, C_4 > 0$ are constants. Collecting all the previous inequalities, we arrive at

$$\begin{aligned} \frac{1}{2}\sum_{i=1}^{N}\sum_{K\in\mathcal{T}} m(K)(u_{i,K}^{M+1})^2 + \frac{1}{2}\sum_{i=1}^{N} d_i \sum_{n=0}^{M}\Delta t \sum_{K\in\mathcal{T}}\sum_{L\in\mathcal{N}(K)} \tau_{K|L}(u_{i,L}^{n+1} - u_{i,K}^{n+1})^2 \\ \leq C_5 + C_2 \sum_{i=1}^{N}\sum_{n=0}^{M}\Delta t \sum_{K\in\mathcal{T}} m(K)(u_{i,K}^{n+1})^2. \end{aligned} \tag{3.8}$$

Using this inequality, we can deduce

$$\sum_{i=1}^{N}\sum_{K\in\mathcal{T}} m(K)(u_{i,K}^{M+1})^2 \leq C_6 + C_7 \sum_{n=0}^{M}\sum_{i=1}^{N}\Delta t \sum_{K\in\mathcal{T}} m(K)(u_{i,K}^{n+1})^2. \tag{3.9}$$

Thus by the discrete Gronwall inequality we obtain from the previous inequality that

$$\sum_{i=1}^{N}\sum_{K\in\mathcal{T}} m(K)(u_{i,K}^{n_0+1})^2 \leq C_8, \tag{3.10}$$

for all $n_0 \in \{1,\dots,M\}$ and some constant $C_8 > 0$, this shows (3.6) and from (3.8) we deduce (3.7). □

3.3. **Compactness argument.** Let us consider a sequence of admissible meshes $(\mathcal{T}_m)_{m\geq 1}$ of Ω such that $\mathrm{size}(\mathcal{T}_m) \to 0$, as $m \to +\infty$ and let $(N_m)_{m\geq 1}$ be an increasing sequence of integers, so we obtain a sequence of time steps $(\Delta t_m)_{m\geq 1}$ such that $\Delta t_m \to 0$, as $m \to +\infty$. We will employ the notation $\boldsymbol{u}_{h_m} = (u_{1,h_m},\dots,u_{N,h_m})^{\mathrm{T}}$ for a piecewise constant solution of (2.13) defined as (2.12). Let us define the translated space $Q_{T-\tau} := \Omega \times (0, T-\tau)$, for all $\tau \in (0,T)$.

Lemma 3.4 (Time-translate estimates)**.** *Let $\Delta t_0 > 0$ small enough. Given a time-step $\Delta t_m \leq \Delta t_0$, then there exists a constant $C > 0$ independent of m and τ such that*

$$\iint_{Q_{T-\tau}} \left|u_{i,h_m}(\boldsymbol{x}, t+\tau) - u_{i,h_m}(\boldsymbol{x},t)\right|^2 \mathrm{d}\boldsymbol{x}\,\mathrm{d}t \leq C(\tau + \Delta t_m), \quad i = 1,\dots,N \tag{3.11}$$

for all $\tau \in (0,T)$.

Proof. Let $i \in \{1,\dots,N\}$ be fixed. We introduce the quantity

$$\mathcal{C}_m(t) = \int_\Omega \left|u_{i,h_m}(\boldsymbol{x}, t+\tau) - u_{i,h_m}(\boldsymbol{x},t)\right|^2 \mathrm{d}\boldsymbol{x}, \quad \text{for all } t \in (0, T-\tau), \tag{3.12}$$

and we set $n_0(t) = [t/\Delta t_m]$ and $n_1(t) = [(t+\tau)/\Delta t_m]$, where $[x] = n$ for $x \in [n, n+1)$, $n \in \mathbb{N}$. We can then rewrite $\mathcal{C}_m(t)$ as

$$\mathcal{C}_m(t) = \sum_{K\in\mathcal{T}_m} m(K)\big(u_{i,K}^{n_1(t)} - u_{i,K}^{n_0(t)}\big)^2 \leq \sum_{K\in\mathcal{T}_m}\Big(\big(u_{i,K}^{n_1(t)} - u_{i,K}^{n_0(t)}\big) \times \sum_{t\leq n\Delta t_m < t+\tau} m(K)(u_{i,K}^{n+1} - u_{i,K}^{n})\Big).$$

Using equation (2.13), Theorem 3.2, summation by parts, along with the weighted Young inequality, we get

$$\begin{aligned} \mathcal{C}_m(t) &\leq d_i \sum_{t\leq n\Delta t_m < t+\tau} \Delta t_m \sum_{K\in\mathcal{T}_m} \big(u_{i,K}^{n_1(t)} - u_{i,K}^{n_0(t)}\big)\left(\sum_{L\in\mathcal{N}(K)} \tau_{K|L}(u_{i,L}^{n+1} - u_{i,K}^{n+1})\right) \\ &\quad + \sum_{t\leq n\Delta t_m < t+\tau} \Delta t_m \sum_{K\in\mathcal{T}_m} m(K)\Big(u_{i,K}^{n_1(t)} - u_{i,K}^{n_0(t)}\Big)\Big(f_i(\boldsymbol{u}_K^n) - g_i(\boldsymbol{u}_K^n)u_{i,K}^{n+1}\Big) \\ &\leq d_i \sum_{t\leq n\Delta t_m < t+\tau} \Delta t_m \sum_{K\in\mathcal{T}_m}\sum_{L\in\mathcal{N}(K)} \tau_{K|L}\left\{(u_{i,L}^{n+1} - u_{i,K}^{n+1}) \times \Big[(u_{i,K}^{n_1(t)} - u_{i,L}^{n_1(t)}) - (u_{i,K}^{n_0(t)} - u_{i,L}^{n_0(t)})\Big]\right\} \end{aligned}$$

$$
\begin{aligned}
&+\sum_{t\le n\Delta t_m<t+\tau}\Delta t_m\sum_{K\in\mathcal{T}_m} m(K)\Big(u_{i,K}^{n_1(t)}f_i(\boldsymbol{u}_K^n)+u_{i,K}^{n_0(t)}g_i(\boldsymbol{u}_K^n)u_{i,K}^{n+1}\Big)\\
&\le \mathcal{C}_{1,m}(t)+\mathcal{C}_{2,m}(t)+\mathcal{C}_{3,m}(t)+\mathcal{C}_{4,m}(t)+\mathcal{C}_{5,m}(t)+\mathcal{C}_{6,m}(t),
\end{aligned}
$$

where we have defined,

$$
\begin{aligned}
\mathcal{C}_{1,m}(t)&=d_i\sum_{t\le n\Delta t_m<t+\tau}\Delta t_m\sum_{K\in\mathcal{T}_m}\sum_{L\in\mathcal{N}(K)}\tau_{K|L}\big|u_{i,L}^{n+1}-u_{i,K}^{n+1}\big|^2,\\
\mathcal{C}_{2,m}(t)&=\frac{d_i}{2}\sum_{t\le n\Delta t_m<t+\tau}\Delta t_m\sum_{K\in\mathcal{T}_m}\sum_{L\in\mathcal{N}(K)}\tau_{K|L}\big|u_{i,L}^{n_1(t)}-u_{i,K}^{n_1(t)}\big|^2,\\
\mathcal{C}_{3,m}(t)&=\frac{d_i}{2}\sum_{t\le n\Delta t_m<t+\tau}\Delta t_m\sum_{K\in\mathcal{T}_m}\sum_{L\in\mathcal{N}(K)}\tau_{K|L}\big|u_{i,L}^{n_0(t)}-u_{i,K}^{n_0(t)}\big|^2,\\
\mathcal{C}_{4,m}(t)&=K_f\sum_{t\le n\Delta t_m<t+\tau}\Delta t_m\sum_{K\in\mathcal{T}_m} m(K)u_{i,K}^{n_1(t)}\\
\mathcal{C}_{5,m}(t)&=K_f\sum_{t\le n\Delta t_m<t+\tau}\Delta t_m\sum_{j=1}^{N}\sum_{K\in\mathcal{T}_m} m(K)u_{i,K}^{n_1(t)}u_{j,K}^{n}\\
\mathcal{C}_{6,m}(t)&=K_g\sum_{t\le n\Delta t_m<t+\tau}\Delta t_m\sum_{K\in\mathcal{T}_m} m(K)u_{i,K}^{n_0(t)}u_{i,K}^{n+1}.
\end{aligned}
\tag{3.13}
$$

We now introduce the characteristic function ζ defined by $\zeta(n,t_1,t_2)=1$, if $t_1<(n+1)\Delta t_m\le t_2$ and $\zeta(n,t_1,t_2)=0$ otherwise. Then, for any sequence $(a^n)_{n\in\mathbb{N}}$ of non-negative numbers we have that

$$
\int_0^{T-\tau}\sum_{t\le n\Delta t_m<t+\tau}a^n\,\mathrm{d}t\le\sum_{n=0}^{\left[\frac{T}{\Delta t_m}\right]}a^n\int_0^{T-\tau}\zeta(n,\tau,t+\tau)\,\mathrm{d}t\le\tau\sum_{n=0}^{\left[\frac{T}{\Delta t_m}\right]}a^n,
\tag{3.14}
$$

and for any $\xi\in[0,\tau]$

$$
\int_0^{T-\tau}\sum_{t\le n\Delta t_m<t+\tau}a^{[(t+\xi)/\Delta t_m]}\,\mathrm{d}t\le\tau\sum_{n=0}^{\left[\frac{T}{\Delta t_m}\right]}a^n.
\tag{3.15}
$$

From (3.14) we deduce that

$$
\begin{aligned}
\int_0^{T-\tau}\mathcal{C}_{1,m}(t)\,\mathrm{d}t&\le\sum_{n=0}^{N_m}\Delta t_m\int_0^{T-\tau}\zeta(n,t,t+\tau)\sum_{K\in\mathcal{T}_m}\sum_{L\in\mathcal{N}(K)}\tau_{K|L}\big|u_{i,L}^{n+1}-u_{i,K}^{n+1}\big|^2\,\mathrm{d}t\\
&\le\tau\sum_{n=0}^{N_m}\Delta t_m\sum_{K\in\mathcal{T}_m}\sum_{L\in\mathcal{N}(K)}\tau_{K|L}\big|u_{i,L}^{n+1}-u_{i,K}^{n+1}\big|^2.
\end{aligned}
$$

In view of the discrete estimate (3.7), there exists a constant $C>0$ such that

$$
\int_0^{T-\tau}\mathcal{C}_{1,m}(t)\,\mathrm{d}t\le\tau C.
\tag{3.16}
$$

Next, we use (3.15) with $\xi=\tau$ for $\mathcal{C}_{2,m}(t)$, and $\xi=0$ for $\mathcal{C}_{3,m}(t)$ to obtain

$$
\int_0^{T-\tau}\mathcal{C}_{2,m}(t)\,\mathrm{d}t\le\tau\sum_{n=0}^{N_m}\Delta t_m\sum_{K\in\mathcal{T}_m}\sum_{L\in\mathcal{N}(K)}\tau_{K|L}\big|u_{i,L}^{n+1}-u_{i,K}^{n+1}\big|^2\le\tau C,
$$

and,

$$
\int_0^{T-\tau}\mathcal{C}_{3,m}(t)\,\mathrm{d}t\le\tau\sum_{n=0}^{N_m}\Delta t_m\sum_{K\in\mathcal{T}_m}\sum_{L\in\mathcal{N}(K)}\tau_{K|L}\big|u_{i,L}^{n+1}-u_{i,K}^{n+1}\big|^2\le\tau C.
$$

Then, we employ (3.15) with $\xi = \tau$ and (3.7) to deduce that

$$\begin{aligned}\int_0^{T-\tau} \mathcal{C}_{4,m}(t)\,\mathrm{d}t &\le \tau K_f \sum_{n=0}^{N_m} \Delta t_m \sum_{K\in\mathcal{T}_m} m(K) u_{i,K}^{n+1} \\ &\le \tau\left(\frac{K_f}{2}\sum_{n=0}^{N_m}\Delta t_m \sum_{K\in\mathcal{T}_m} m(K)\big(u_{i,K}^{n+1}\big)^2\right) + \tau\left(\frac{K_f}{2}\sum_{n=0}^{N_m}\Delta t_m \sum_{K\in\mathcal{T}_m} m(K)\right) \\ &\le \tau C.\end{aligned} \tag{3.17}$$

Now, for the estimate $\mathcal{C}_{5,m}(t)$ we first use Young's inequality to get

$$\begin{aligned}\mathcal{C}_{5,m}(t) &\le K_f \sum_{t\le n\Delta t_m < t+\tau} \Delta t_m \sum_{j=1}^{N}\sum_{K\in\mathcal{T}_m} m(K) u_{i,K}^{n_1(t)} u_{j,K}^n \\ &\le \frac{K_f N}{2}\sum_{t\le n\Delta t_m<t+\tau}\Delta t_m \sum_{K\in\mathcal{T}_m} m(K)\big(u_{i,K}^{n_1(t)}\big)^2 + \frac{K_f}{2}\sum_{t\le n\Delta t_m<t+\tau}\Delta t_m \sum_{j=1}^{N}\sum_{K\in\mathcal{T}_m} m(K)(u_{j,K}^n)^2.\end{aligned}$$

Then, in the first sum above, we employ (3.14) with $\xi = 0$, while in the second sum, we apply (3.15). Combining these with (3.6), we obtain

$$\begin{aligned}\int_0^{T-\tau}\mathcal{C}_{5,m}(t)\,\mathrm{d}t &\le \tau\frac{K_f N}{2}\sum_{n=0}^{N_m}\Delta t_m\sum_{K\in\mathcal{T}_m} m(K)\big(u_{i,K}^{n+1}\big)^2 + \tau\frac{K_f}{2}\sum_{n=0}^{N_m}\Delta t_m\sum_{j=1}^{N}\sum_{K\in\mathcal{T}_m} m(K)(u_{j,K}^n)^2 \\ &\le \tau C.\end{aligned}$$

Proceeding in a similar way, we obtain for $\mathcal{C}_{6,m}(t)$ that

$$\int_0^{T-\tau}\mathcal{C}_{6,m}(t)\,\mathrm{d}t \le \tau C, \tag{3.18}$$

for some constant $C > 0$. This ends the proof of the time translate estimate. □

Lemma 3.5 (Space translate estimates)**.** *Let $\Delta t_0 > 0$ be small enough. Given a time-step $\Delta t_m \le \Delta t_0$, then there exists a constant $C > 0$ independent of m and τ such that, for all $\boldsymbol{y} \in \mathbb{R}^2$,*

$$\int_0^T\int_{\Omega_{\boldsymbol{y}}} \big|u_{i,h_m}(\boldsymbol{x}+\boldsymbol{y},t) - u_{i,h_m}(\boldsymbol{x},t)\big|^2\,\mathrm{d}\boldsymbol{x}\,\mathrm{d}t \le C\|\boldsymbol{y}\|_2\big(\|\boldsymbol{y}\|_2 + 2(K_\Omega - 1)h_m\big), \tag{3.19}$$

for $i = 1,\dots,N$, where $\Omega_{\boldsymbol{y}} = \{\boldsymbol{x}\in\Omega : \boldsymbol{x}+\boldsymbol{y}\in\Omega\}$ and K_Ω is the number of sides of Ω.

Proof. To establish this result, we follow the approach of Lemma 9.3 in Eymard et al. [24], to obtain

$$\begin{aligned}&\int_0^T\int_{\Omega_{\boldsymbol{y}}} \big|u_{i,h_m}(\boldsymbol{x}+\boldsymbol{y},t) - u_{i,h_m}(\boldsymbol{x},t)\big|^2\,\mathrm{d}\boldsymbol{x}\,\mathrm{d}t \\ &\qquad\le \|\boldsymbol{y}\|_2\big(\|\boldsymbol{y}\|_2 + 2(K_\Omega-1)h_m\big)\sum_{n=0}^{N_m}\Delta t_m\sum_{K\in\mathcal{T}_m}\sum_{L\in\mathcal{N}(K)}\tau_{K|L}\big|u_{i,L}^{n+1} - u_{i,K}^{n+1}\big|^2,\end{aligned}$$

for $i = 1,\dots,N$. Using the estimate (3.7), one can obtain the space translate estimate (3.19). This ends the proof of the lemma. □

3.4. **Convergence analysis.**

Theorem 3.6 (Convergence Towards a Weak Solution)**.** *Assume that $\boldsymbol{u}^0 = (u_1^0,\dots,u_N^0)^{\mathrm{T}}$ is such that $u_i^0 \in H^1(\Omega)$, for $i = 1,\dots,N$ and $\boldsymbol{u}^0(\boldsymbol{x}) \in \mathbb{R}_+^N$, for a.e. $\boldsymbol{x}\in\Omega$. Let $(\boldsymbol{u}_{h_m})_{m\ge1}$ be a family of solutions such that $h_m \to 0$, as $m\to\infty$. There exists $u_i \in L^2(0,T;H^1(\Omega))$, $i = 1,\dots,N$ such that, up to a subsequence*

a) $u_{i,h_m} \longrightarrow u_i$ strongly in $L^p(\Omega_T)$ and a.e. in Ω_T as $m\to\infty$, for all $1\le p<\infty$, $i = 1,\dots,N$.
b) $\nabla_{\mathcal{T}_m} u_{i,h_m} \rightharpoonup \nabla u_i$, weakly in $[L^2(\Omega_T)]^2$ as $m\to\infty$, for $i = 1,\dots,N$.

c) Moreover, the limit $\boldsymbol{u} = (u_1, \dots, u_N)^{\mathrm{T}}$ *is a weak solution (in the sense of Definition 3.1) of the problem* (1.1).

Proof. Let $i \in \{1, \dots, N\}$ be fixed. To show *a)*, we apply Kolmogorov's compactness criterion (see [24], Theorem 14.1) as a tool to analyze the sequence $(u_{i,h_m})_{m\in\mathbb{N}}$. To do so, we define $N = 3$, $q = 2$, and $p(u_{i,h_m}) = \hat{u}_{i,h_m}$, where $\hat{u}_i$ is defined by $\hat{u}_{i,h_m} = u_{i,h_m}$ within Ω_T and $\hat{u}_{i,h_m} = 0$ outside of Ω_T. The first condition of Kolmogorov's compactness criterion is guaranteed by the definition of $\hat{u}_i$ and the second condition follows from Lemma 3.3. Thus, to complete the proof, it remains to verify the third condition of Kolmogorov's theorem. Now, for any $\boldsymbol{y} \in \mathbb{R}^2$ and $\tau \in \mathbb{R}$, the triangle inequality yields

$$\begin{aligned}\left\|\hat{u}_{i,h_m}(\cdot+\boldsymbol{y},\cdot+\tau) - \hat{u}_{i,h_m}(\cdot,\cdot)\right\|_{L^2(\mathbb{R}^N)} &\le \left\|\hat{u}_{i,h_m}(\cdot+\boldsymbol{y},\cdot+\tau) - \hat{u}_{i,h_m}(\cdot+\boldsymbol{y},\cdot)\right\|_{L^2(\mathbb{R}^N)} \\ &\quad + \left\|\hat{u}_{i,h_m}(\cdot+\boldsymbol{y},\cdot) - \hat{u}_{i,h_m}(\cdot,\cdot)\right\|_{L^2(\mathbb{R}^N)}.\end{aligned}$$

Thanks to the translate estimates given by Lemma 3.4 and 3.5 we have that

$$\left\|\hat{u}_{i,h_m}(\cdot+\boldsymbol{y},\cdot+\tau) - \hat{u}_{i,h_m}(\cdot,\cdot)\right\|_{L^2(\mathbb{R}^N)} \longrightarrow 0,$$

as $\boldsymbol{y} \to 0$ and $\tau \to 0$. This guarantees the compactness of the sequence $(u_{i,h_m})_m$ in $L^2(\Omega_T)$. Then, using the Kolmogorov theorem, there exists a subsequence still denoted by $(u_{i,h_m})_m$, and a function $u_i \in L^2(\Omega_T)$ such that $u_{i,h_m} \longrightarrow u_i$ strongly in $L^2(\Omega_T)$ and a.e. in Ω_T. Since this sequence is bounded in $L^\infty(\Omega_T)$, this convergence also holds in $L^p(\Omega_T)$, for all $p \in [1, +\infty)$. This concludes the proof of *(a)*.
We now proceed to establish item *b)*. Using the discrete estimate (3.7), we can establish that the sequence $\left(\nabla_{\mathcal{T}_m} u_{i,h_m}\right)_m$ is uniformly bounded in $[L^2(\Omega_T)]^2$. Therefore, up to a possibly unlabeled subsequence, this sequence converges weakly to a function $p_i^* \in [L^2(\Omega_T)]^2$. Then, we identify ∇u_i by p_i^* by using the following convergence result (see, e.g., [12, 15])

$$\int_0^T \int_\Omega \left(\nabla_{\mathcal{T}_m} u_{i,h_m} \cdot \phi_i + u_{i,h_m} \nabla \cdot \phi_i\right) \mathrm{d}\boldsymbol{x}\, \mathrm{d}t \longrightarrow 0, \quad \text{as } m \to +\infty, \quad \forall \phi_i \in [\mathcal{D}(\Omega_T)]^2.$$

This ends the proof of *c)*.
Finally, we establish *(d)*, that is, we identify the function $\boldsymbol{u} = (u_1, \dots, u_N)^{\mathrm{T}}$, obtained from the arguments above, as a weak solution of the continuous problem (1.1) in the sense of Definition 3.1. Let $i \in \{1, \dots, N\}$ be fixed. We consider $\psi \in \mathcal{D}(\overline{\Omega} \times [0, T))$ and denote by $\psi_K^n = \psi(\boldsymbol{x}_K, t_n)$, for all $K \in \mathcal{T}$ and $n \in \{0, \dots, N_m\}$. Multiplying equation (2.13) by $\Delta t_m \psi_K^{n+1}$ and summing over $K \in \mathcal{T}_m$ and $n \in \{0, \dots, N_m\}$ yields $A_m + B_m = C_m + D_m$, where

$$\begin{aligned}
A_m &= \sum_{n=0}^{N_m} \sum_{K\in\mathcal{T}_m} m(K)(u_{i,K}^{n+1} - u_{i,K}^n)\psi_K^{n+1}, \\
B_m &= -d_i \sum_{n=0}^{N_m} \Delta t_m \sum_{K\in\mathcal{T}_m} \sum_{L\in\mathcal{N}(K)} \tau_{K|L}(u_{i,L}^{n+1} - u_{i,K}^{n+1})\psi_K^{n+1}, \\
C_m &= \sum_{n=0}^{N_m} \Delta t_m \sum_{K\in\mathcal{T}_m} m(K) f_i(\boldsymbol{u}_K^n)\psi_K^{n+1}, \\
D_m &= -\sum_{n=0}^{N_m} \Delta t_m \sum_{K\in\mathcal{T}_m} m(K) g_i(\boldsymbol{u}_K^n) u_{i,K}^{n+1}\psi_K^{n+1}.
\end{aligned} \tag{3.20}$$

Then, using summation by parts in time and noticing that $\psi_K^{N_m+1} = 0$, for all $K \in \mathcal{T}_m$ we get

$$\begin{aligned}
A_m &= -\sum_{n=0}^{N_m} \sum_{K\in\mathcal{T}_m} m(K) u_{i,K}^{n+1}(\psi_K^{n+1} - \psi_K^n) - \sum_{K\in\mathcal{T}_m} m(K) u_{i,K}^0 \psi_K^0 \\
&= -\iint_{\Omega_T} u_{i,h_m}(\boldsymbol{x}, t)\partial_t \psi(\boldsymbol{x}_K, t)\, \mathrm{d}\boldsymbol{x}\, \mathrm{d}t - \int_\Omega u_{i,0}(\boldsymbol{x})\psi(\boldsymbol{x}_K, 0)\, \mathrm{d}\boldsymbol{x} := -A_m^{(1)} - A_m^{(2)}.
\end{aligned} \tag{3.21}$$

Then, using the regularity properties of ψ, we obtain

$$\begin{aligned}\left|A_m^{(1)} - \iint_{\Omega_T} u_i(\boldsymbol{x},t)\partial_t\psi(\boldsymbol{x},t)\,\mathrm{d}\boldsymbol{x}\,\mathrm{d}t\right| &= \iint_{\Omega_T} \left|u_{i,h_m}(\boldsymbol{x},t)\partial_t\psi(\boldsymbol{x}_K,t) - u_i(\boldsymbol{x},t)\partial_t\psi(\boldsymbol{x},t)\right|\mathrm{d}\boldsymbol{x}\,\mathrm{d}t\\ &\le \iint_{\Omega_T} \left|u_{i,h_m}(\boldsymbol{x},t)\right|\left|\partial_t\psi(\boldsymbol{x}_K,t) - \partial_t\psi(\boldsymbol{x},t)\right|\mathrm{d}\boldsymbol{x}\,\mathrm{d}t\\ &\quad + \iint_{\Omega_T} \left|u_{i,h_m}(\boldsymbol{x},t)\partial_t\psi(\boldsymbol{x},t) - u_i(\boldsymbol{x},t)\partial_t\psi(\boldsymbol{x},t)\right|\mathrm{d}\boldsymbol{x}\,\mathrm{d}t\\ &\le \frac{1}{2}\|u_{i,h_m}\|_{0,\Omega_T}^2\sqrt{h_m} + \frac{m(\Omega_T)}{2}\|\partial_{xt}\psi\|_{\infty,\Omega_T}^2\sqrt{h_m}\\ &\quad + \iint_{\Omega_T} \left|u_{i,h_m}(\boldsymbol{x},t)\partial_t\psi(\boldsymbol{x},t) - u_i(\boldsymbol{x},t)\partial_t\psi(\boldsymbol{x},t)\right|\mathrm{d}\boldsymbol{x}\,\mathrm{d}t.\end{aligned}$$

Thus, using the regularity of the function ψ, the boundedness of the sequence $(u_{i,h_m})_m$ in $L^2(\Omega_T)$, and the weak convergence in $L^2(\Omega_T)$ of u_{i,h_m} towards u_i it follows that

$$A_m^{(1)} \longrightarrow \iint_{\Omega_T} u_i(\boldsymbol{x},t)\partial_t\psi(\boldsymbol{x},t)\,\mathrm{d}\boldsymbol{x}\,\mathrm{d}t, \quad \text{as } m\to+\infty. \tag{3.22}$$

In the same way, using the Lipschitz continuity of the function ψ, we observe that

$$\begin{aligned}\left|A_m^{(2)} - \int_\Omega u_i^0(\boldsymbol{x})\psi(\boldsymbol{x},0)\,\mathrm{d}\boldsymbol{x}\right| &\le \int_\Omega |u_i^0(\boldsymbol{x})||\psi(\boldsymbol{x}_K,0) - \psi(\boldsymbol{x},0)|\,\mathrm{d}\boldsymbol{x}\\ &\le \frac{1}{2}\|u_i^0\|_{0,\Omega}^2\sqrt{h_m} + \frac{m(\Omega)}{2}\|\partial_x\psi\|_{\infty,\Omega_T}^2\sqrt{h_m}.\end{aligned}$$

This yields

$$A_m^{(2)} \longrightarrow \int_\Omega u_i^0(\boldsymbol{x})\psi(\boldsymbol{x},0)\,\mathrm{d}\boldsymbol{x}, \quad \text{as } m\to+\infty. \tag{3.23}$$

From (3.21), (3.22), and (3.23) it follows that

$$A_m \longrightarrow -\iint_{\Omega_T} u_i(\boldsymbol{x},t)\partial_t\psi(\boldsymbol{x},t)\,\mathrm{d}\boldsymbol{x}\,\mathrm{d}t - \int_\Omega u_i^0(\boldsymbol{x})\psi(\boldsymbol{x},0)\,\mathrm{d}\boldsymbol{x}, \quad \text{as } m\to+\infty. \tag{3.24}$$

Now, we focus on the diffusive part B_m. We define $\psi_{h_m}(\boldsymbol{x},t) = \psi_K^n$, for all $\boldsymbol{x}\in K$ and $t\in[t_n,t_{n+1})$, then integrate by parts, and, taking into account that $\tau_{K|L} = 2m(T_{KL})/d_{K|L}^2$, we use the definition of the discrete gradient (2.11) to obtain

$$\begin{aligned}B_m &= d_i\sum_{n=0}^{N_m}\Delta t_m \sum_{K\in\mathcal{T}_m}\sum_{L\in\mathcal{N}(K)} \tau_{K|L}(u_{i,L}^{n+1} - u_{i,K}^{n+1})(\psi_L^{n+1} - \psi_K^{n+1})\\ &= \frac{d_i}{2}\sum_{n=0}^{N_m}\Delta t_m \sum_{K\in\mathcal{T}_m}\sum_{L\in\mathcal{N}(K)} m(T_{KL})\left[2\left(\frac{u_{i,L}^{n+1} - u_{i,K}^{n+1}}{d_{K|L}}\right)\cdot\boldsymbol{n}_{K|L}\right]\left[2\left(\frac{\psi_L^{n+1} - \psi_K^{n+1}}{d_{K|L}}\right)\cdot\boldsymbol{n}_{K|L}\right]\\ &= \frac{d_i}{2}\sum_{n=0}^{N_m}\Delta t_m \int_\Omega \nabla_{\mathcal{T}_m} u_{i,\mathcal{T}_m}^{n+1}\cdot\nabla_{\mathcal{T}_m}\psi_{\mathcal{T}_m}^{n+1}\,\mathrm{d}\boldsymbol{x}.\end{aligned} \tag{3.25}$$

Now, let us define $\boldsymbol{x}_{KL} = \theta\boldsymbol{x}_K + (1-\theta)\boldsymbol{x}_L$, for $0<\theta<1$ some point of the segment $[\![\boldsymbol{x}_K,\boldsymbol{x}_L]\!]$ such that

$$\psi(\boldsymbol{x}_L,t_{n+1}) - \psi(\boldsymbol{x}_K,t_{n+1}) = d_{K|L}\nabla\psi(\boldsymbol{x}_{KL},t_{n+1})\cdot\boldsymbol{n}_{K|L}.$$

Then one gets

$$\nabla_{\mathcal{T}_m}\psi_{\mathcal{T}_m}^{n+1} = 2\left(\frac{\psi_L^{n+1} - \psi_K^{n+1}}{d_{K|L}}\right)\cdot\boldsymbol{n}_{K|L} = 2\left(\frac{\psi(\boldsymbol{x}_L,t_{n+1}) - \psi(\boldsymbol{x}_K,t_{n+1})}{d_{K|L}}\right)\cdot\boldsymbol{n}_{K|L} = 2\nabla\psi(\boldsymbol{x}_{KL},t_{n+1}).$$

Let us define $(\nabla\psi)_{h_m}(\boldsymbol{x},t) = \nabla\psi(\boldsymbol{x}_{KL},t_{n+1})$, for all $(\boldsymbol{x},t)\in T_{KL}\times(t_n,t_{n+1})$. Then from (3.25) it follows that

$$B_m = d_i \iint_{\Omega_T} \nabla_{\mathcal{T}_m} u_{i,\mathcal{T}_m}(\boldsymbol{x},t)\cdot(\nabla\psi)_{h_m}(\boldsymbol{x},t)\,\mathrm{d}\boldsymbol{x}. \tag{3.26}$$

Now, by employing the weak convergence *c)* of the discrete gradient of u_{i,h_n} and the regularity properties of the test function ψ allow us to deduce that

$$B_m \longrightarrow d_i \iint_{\Omega_T} \nabla u_i(\boldsymbol{x},t)\cdot\nabla\psi(\boldsymbol{x},t)\,\mathrm{d}\boldsymbol{x}\,\mathrm{d}t, \quad \text{as } m\to+\infty. \tag{3.27}$$

For the reaction terms C_m and D_m, we observe that

$$\begin{aligned} C_m &= \iint_{\Omega_T} f_i\big(\boldsymbol{u}_{h_m}(\boldsymbol{x},t-\Delta t_m)\big)\psi_{h_m}(\boldsymbol{x},t)\,\mathrm{d}\boldsymbol{x}\,\mathrm{d}t,\\ D_m &= -\iint_{\Omega_T} g_i\big(\boldsymbol{u}_{h_m}(\boldsymbol{x},t-\Delta t_m)\big)u_{i,h_m}(\boldsymbol{x},t)\psi_{h_m}(\boldsymbol{x},t)\,\mathrm{d}\boldsymbol{x}\,\mathrm{d}t, \end{aligned}$$

where we have defined $u_{i,h_m}(\boldsymbol{x},t-\Delta t_m) = u_{i,h_m}(\boldsymbol{x},t)$, for all $t\in[0,\Delta t_m]$. Then, employing the triangle and Cauchy-Schwarz inequalities, the regularity of the function ψ and the time-translate estimate (3.11), we arrive at

$$\begin{aligned} \left|C_m - \iint_{\Omega_T} f_i(\boldsymbol{u}(\boldsymbol{x},t))\psi(\boldsymbol{x},t)\,\mathrm{d}\boldsymbol{x}\,\mathrm{d}t\right| &\le \iint_{\Omega_T} \big|f_i\big(\boldsymbol{u}_{h_m}(\boldsymbol{x},t-\Delta t_m)\big)\big|\big|\psi_{h_m}(\boldsymbol{x},t)-\psi(\boldsymbol{x},t)\big|\mathrm{d}\boldsymbol{x}\,\mathrm{d}t\\ &\quad + \iint_{\Omega_T} \big|f_i\big(\boldsymbol{u}_{h_m}(\boldsymbol{x},t-\Delta t_m)\big) - f_i\big(\boldsymbol{u}(\boldsymbol{x},t)\big)\big|\big|\psi(\boldsymbol{x},t)\big|\,\mathrm{d}\boldsymbol{x}\,\mathrm{d}t\\ &\le K_f \iint_{\Omega_T}\left(1+\sum_{j=1}^{N}\big|u_{j,h_m}(\boldsymbol{x},t)\big|\right)\big|\psi_{h_m}(\boldsymbol{x},t)-\psi(\boldsymbol{x},t)\big|\,\mathrm{d}\boldsymbol{x}\,\mathrm{d}t\\ &\quad + L_f \iint_{\Omega_T} |u_{i,h_m}(\boldsymbol{x},t-\Delta t_m)-u_{i,h_m}(\boldsymbol{x},t)||\psi(\boldsymbol{x},t)|\,\mathrm{d}\boldsymbol{x}\,\mathrm{d}t\\ &\le K_f\sqrt{m(\Omega_T)}\|\psi_{h_m}-\psi\|_{0,\Omega_T} + K_f\sum_{j=1}^{N}\|u_{j,h_m}\|_{0,\Omega_T}\|\psi_{h_m}-\psi\|_{0,\Omega_T}\\ &\quad + L_f\left(\iint_{\Omega_T}|u_{i,h_m}(\boldsymbol{x},t-\Delta t_m)-u_{i,h_m}(\boldsymbol{x},t)|^2\,\mathrm{d}\boldsymbol{x}\,\mathrm{d}t\right)^{1/2}\|\psi\|_{0,\Omega_T}\\ &\le K_f\sqrt{m(\Omega_T)}\|\psi_{h_m}-\psi\|_{0,\Omega_T} + K_f\sum_{j=1}^{N}\|u_{j,h_m}\|_{0,\Omega_T}\|\psi_{h_m}-\psi\|_{0,\Omega_T}\\ &\quad + C\sqrt{\Delta t_m}\|\psi\|_{0,\Omega_T}. \end{aligned}$$

Thus, we can deduce that

$$C_m \longrightarrow \iint_{\Omega_T} f_i\big(\boldsymbol{u}(\boldsymbol{x},t)\big)\psi(\boldsymbol{x},t)\,\mathrm{d}\boldsymbol{x}\,\mathrm{d}t, \quad \text{as } m\to+\infty. \tag{3.28}$$

In a similar way, for the reaction term D_m we have used the triangle and Cauchy-Schwarz inequalities, the regularity of the function ψ and the time-translate estimate (3.11), to obtain

$$\begin{aligned}
&\left|D_m - \iint_{\Omega_T} g_i(\boldsymbol{u}(\boldsymbol{x},t))u_i(\boldsymbol{x},t)\psi(\boldsymbol{x},t)\,\mathrm{d}\boldsymbol{x}\,\mathrm{d}t\right| \\
&\quad\le \iint_{\Omega_T} |g_i(\boldsymbol{u}_{h_m}(\boldsymbol{x},t-\Delta t_m)) - g_i(\boldsymbol{u}(\boldsymbol{x},t))||u_{i,h_m}(\boldsymbol{x},t)||\psi_{h_m}(\boldsymbol{x},t)|\,\mathrm{d}\boldsymbol{x}\,\mathrm{d}t \\
&\qquad + \iint_{\Omega_T} |g_i(\boldsymbol{u}(\boldsymbol{x},t))||u_{i,h_m}(\boldsymbol{x},t) - u_i(\boldsymbol{x},t)||\psi_{h_m}(\boldsymbol{x},t)|\,\mathrm{d}\boldsymbol{x}\,\mathrm{d}t \\
&\qquad + \iint_{\Omega_T} |g_i(\boldsymbol{u}(\boldsymbol{x},t))||u_i(\boldsymbol{x},t)||\psi_{h_m}(\boldsymbol{x},t) - \psi(\boldsymbol{x},t)|\,\mathrm{d}\boldsymbol{x}\,\mathrm{d}t \\
&\quad\le L_g\|\psi_{h_m}\|_{\infty,\Omega_T} \iint_{\Omega_T} |\boldsymbol{u}_{h_m}(\boldsymbol{x},t-\Delta t_m) - \boldsymbol{u}(\boldsymbol{x},t)||u_{i,h_m}(\boldsymbol{x},t)|\,\mathrm{d}\boldsymbol{x}\,\mathrm{d}t \\
&\qquad + K_g \iint_{\Omega_T} |u_{i,h_m}(\boldsymbol{x},t) - u_i(\boldsymbol{x},t)||\psi_{h_m}(\boldsymbol{x},t)|\,\mathrm{d}\boldsymbol{x}\,\mathrm{d}t \\
&\qquad + K_g \iint_{\Omega_T} |u_i(\boldsymbol{x},t)||\psi_{h_m}(\boldsymbol{x},t) - \psi(\boldsymbol{x},t)|\,\mathrm{d}\boldsymbol{x}\,\mathrm{d}t \\
&\quad\le L_g\|\psi_{h_m}\|_{\infty,\Omega_T} \left(\iint_{\Omega_T} |\boldsymbol{u}_{h_m}(\boldsymbol{x},t-\Delta t_m) - \boldsymbol{u}(\boldsymbol{x},t)|^2\,\mathrm{d}\boldsymbol{x}\,\mathrm{d}t\right)^{1/2} \|u_{i,h_m}\|_{0,\Omega_T} \\
&\qquad + K_g\|u_{i,h_m} - u_i\|_{0,\Omega_T}\|\psi_{h_m}\|_{0,\Omega_T} + K_g\|u_i\|_{0,\Omega_T}\|\psi_{h_m} - \psi\|_{0,\Omega} \\
&\quad\le L_g\|\psi_{h_m}\|_{\infty,\Omega_T}\sqrt{\Delta t_m}\|u_{i,h_m}\|_{0,\Omega_T} + K_g\|u_{i,h_m} - u_i\|_{0,\Omega_T}\|\psi_{h_m}\|_{0,\Omega_T} + K_g\|u_i\|_{0,\Omega_T}\|\psi_{h_m} - \psi\|_{0,\Omega}.
\end{aligned}$$

Hence, we can conclude that

$$D_m \longrightarrow \iint_{\Omega_T} g_i\big(\boldsymbol{u}(\boldsymbol{x},t)\big)u_i(\boldsymbol{x},t)\psi(\boldsymbol{x},t)\,\mathrm{d}\boldsymbol{x}\,\mathrm{d}t, \quad \text{as } m\to+\infty. \tag{3.29}$$

From (3.24),(3.27), (3.28), and (3.29), it follows that u_i satisfies (3.1). This concludes the proof. □

4. A second-order numerical scheme

The goal of this section is to propose a positivity-preserving scheme that is dynamically consistent with respect to the spatially homogeneous model $\boldsymbol{u}_t = \boldsymbol{F}(\boldsymbol{u})$, and that is also second order in both space and time. Our first step is to design a second-order scheme for the reaction system, which will be based on some recent work by Hoang et al. [31, 32, 34].

4.1. Second Order NSFD scheme for the spatially homogeneous model.

It is well known that the choice of denominator functions like the ones in equation (2.3) leads to first-order schemes [20]. To overcome this, let us follow [32] and define denominator functions that depend not only on Δt but also on the approximations of the state variables: $\boldsymbol{u}_i$, $i = 1,\dots,N$. This modification allows us to obtain a higher order of convergence in the NSFD method, which is described below. Thus, the scheme now reads

$$u_i^{n+1} = \frac{u_i^n + \varphi_i(\Delta t,\boldsymbol{u}^n)f_i(\boldsymbol{u}^n)}{1+\varphi_i(\Delta t,\boldsymbol{u}^n)g_i(\boldsymbol{u}^n)}, \quad i = 1,\dots,N. \tag{4.1}$$

where the denominator function is chosen satisfying the following conditions:

$$\frac{\partial^2\varphi_i}{\partial\Delta t^2}(0,\boldsymbol{u}) = 2g_i(\boldsymbol{u}) + \sum_{j=1}^{N}\frac{\partial F_i}{\partial u_j}(\boldsymbol{u})\frac{F_j(\boldsymbol{u})}{F_i(\boldsymbol{u})}, \tag{4.2}$$

for all $\boldsymbol{u}\in\Sigma$ and $F_i(\boldsymbol{u})\neq 0$, $i = 1,\dots,N$. We emphasize that the conditions appearing on the right-hand side of (4.2) are imposed to ensure the validity of the Taylor expansion, with respect to the variable Δt, of the right-hand-side functions in (2.7). Consequently, there is limited freedom in this regard. Nevertheless,

Algorithm 1 NSFD-2 scheme for $\boldsymbol{u}_t = \boldsymbol{F}(\boldsymbol{u})$

Require: model parameters, N, T, $\Delta t, u_i^0$, $i = 1, \dots, N$
  $u_i^n \leftarrow u_i^0$, $i = 1, \dots, N$
  $M \leftarrow \lceil \frac{T}{\Delta t} \rceil$
  for $n = 1, \dots, M-1$ **do**
    compute $g_i(\boldsymbol{u}^n)$, $i = 1, \dots, N$ given $\boldsymbol{u}^n$
    $\tau_i \leftarrow 2g_i + \sum_{j=1}^{N} \frac{\partial F_j}{\partial u_j} \cdot \frac{F_j}{F_i}$, $i = 1, \dots, N$
    compute $\varphi_i(\Delta t, \boldsymbol{x}^n)$ from (4.3) or (4.4) given Δt, $\boldsymbol{u}^n, \tau_i$, $i = 1, \dots, N$
    $u_i^{n+1} \leftarrow \dfrac{u_i^n + \varphi_i(\Delta t, \boldsymbol{u}^n) f_i(\boldsymbol{u}^n)}{1 + \varphi_i(\Delta t, \boldsymbol{u}^n) g_i(\boldsymbol{u}^n)}, \quad i = 1, \dots, N$
  end for
Ensure: $\{(u_1^1, \dots, u_N^1), \dots, (u_1^M, \dots, u_N^M)\}$

the functions φ_i satisfying these conditions are not uniquely determined. For instance, if τ_i denotes the right-hand side of the i-th equation in (4.2), one possible choice is the exponential-like functions

$$\varphi_i(\Delta t, \boldsymbol{u}) = \begin{cases} \dfrac{e^{\tau_i(\boldsymbol{u})\Delta t} - 1}{\tau_i(\boldsymbol{u})}, & \text{if } \tau_i(\boldsymbol{u}) \neq 0, \\ \Delta t, & \text{if } \tau_i(\boldsymbol{u}) = 0. \end{cases} \tag{4.3}$$

Another possible choice is the polynomial-like functions

$$\varphi_i(\Delta t, \boldsymbol{u}) = \Delta t + \frac{\Delta t^2}{2} \tau_i(\boldsymbol{u}). \tag{4.4}$$

The functions (4.3) and (4.4) satisfy not only (4.2) but also condition (1) in Definition 2.1, i.e., $\varphi_i(\Delta t, \boldsymbol{x}) = \Delta t + \mathcal{O}(\Delta t^2)$, as $\Delta t \to 0$ and $\varphi_i(\Delta t, \boldsymbol{u}) > 0$, for all $\Delta t > 0$ and $\boldsymbol{u} \in \Sigma$. We will refer to this method as NSFD-2 scheme. We notice that at each time step we need to compute the values τ_i and then update the denominator functions φ_i such that conditions (4.2) are fulfilled. The final form of the NSFD-2 scheme is described in Algorithm 1.

Theorem 4.1. *Let $\varphi_i(\Delta t, \boldsymbol{u})$, be functions satisfying the conditions* (4.2)*. Then, NSFD method* (2.6) *is convergent of order* 2*.*

Proof. First, we apply Taylor's theorem to the components of the solution $u_i(t)$, $i = 1, \dots, N$ to obtain

$$u_i(t^{n+1}) = u_i(t^n) + \Delta t u'(t^n) + \frac{\Delta t^2}{2} u_i''(t^n) + \tau_i^n, \tag{4.5}$$

where

$$\tau_i^n = \frac{\Delta t^3}{6} \frac{d^3 u_i}{dt^3}(t^n + \theta_i \Delta t), \quad \theta_i \in [0, 1]. \tag{4.6}$$

are the local truncation errors. If $\boldsymbol{\tau}^n := (\tau_1^n, \dots, \tau_N^n)^{\mathrm{T}}$, then the norm of the local truncation error is $\|\boldsymbol{\tau}^n\|_\infty = \max_{1 \leq i \leq N} \tau_i^n$. By Assumptions (1.2), we have that the right-hand side functions are of class C^2, so it follows that the solution is of class C^3 with bounded derivatives over $[0, T]$. Therefore, we have the following bound for the local truncation error:

$$\|\boldsymbol{\tau}^n\|_\infty \leq M \Delta t^3. \tag{4.7}$$

We now employ the notation $(R_1(\Delta t, \boldsymbol{u}^n), \dots, R_N(\Delta t, \boldsymbol{u}^n))^{\mathrm{T}}$ for the right-hand side of the scheme (2.7). It follows from (2.8) that

$$R_i(0, \boldsymbol{x}) = u_i, \quad i = 1, \dots, N. \tag{4.8}$$

In addition, we observe that the first partial derivative of R_i with respect to Δt is given by

$$\begin{aligned}\frac{\partial R_i(\Delta t,\boldsymbol{u})}{\partial \Delta t} &= \frac{\partial}{\partial \Delta t}\big[u_i + G_i(\Delta t,\boldsymbol{u})F_i(\boldsymbol{u})\big] \\ &= \left[\frac{\partial \varphi_i(\Delta t,\boldsymbol{u})}{\partial \Delta t}\left(\frac{1}{1+\varphi_i(\Delta t,\boldsymbol{u})g_i(\boldsymbol{u})}\right) + \varphi_i(\Delta t,\boldsymbol{u})\left(\frac{-\dfrac{\partial \varphi_i(\Delta t,\boldsymbol{u})}{\partial \Delta t}g_i(\boldsymbol{u})}{(1+\varphi_i(\Delta t,\boldsymbol{u})g_i(\boldsymbol{u}))^2}\right)\right]F_i(\boldsymbol{u}).\end{aligned} \tag{4.9}$$

Then, taking into account that $\varphi_i(0,\boldsymbol{u}) = 0$ and $\frac{\partial \varphi_i(0,\boldsymbol{u})}{\partial \Delta t} = 1$, it follows that

$$\frac{\partial R_i(0,\boldsymbol{u})}{\partial \Delta t} = F_i(\boldsymbol{u}), \quad i = 1,\dots,N. \tag{4.10}$$

Now, from (4.9) we can compute the second derivative of R_i by

$$\begin{aligned}\frac{\partial^2 R_i(\Delta t,\boldsymbol{u})}{\partial \Delta t^2} = \Bigg[&\frac{\partial^2 \varphi_i(\Delta t,\boldsymbol{u})}{\partial \Delta t^2}\left(\frac{1}{1+\varphi_i(\Delta t,\boldsymbol{u})g_i(\boldsymbol{u})}\right) - 2\frac{\partial \varphi_i(\Delta t,\boldsymbol{u})}{\partial \Delta t}\frac{g_i(\boldsymbol{u})}{(1+\varphi_i(\Delta t,\boldsymbol{u})g_i(\boldsymbol{u}))^2} \\ &+\varphi_i(\Delta t,\boldsymbol{u})\frac{\partial}{\partial \Delta t}\left(\frac{-\dfrac{\partial \varphi_i(\Delta t,\boldsymbol{u})}{\partial \Delta t}g_i(\boldsymbol{u})}{(1+\varphi_i(\Delta t,\boldsymbol{u})g_i(\boldsymbol{u}))^2}\right)\Bigg]F_i(\boldsymbol{u}).\end{aligned}$$

Again we use the facts $\varphi_i(0,\boldsymbol{u}) = 0$ and $\frac{\partial \varphi_i(0,\boldsymbol{u})}{\partial \Delta t} = 1$, to obtain

$$\frac{\partial^2 R_i(0,\boldsymbol{u})}{\partial \Delta t^2} = F_i(\boldsymbol{u})\left[\frac{\partial^2 \varphi_i(0,\boldsymbol{u})}{\partial \Delta t^2} - 2g_i(\boldsymbol{u})\right], \quad i = 1,\dots,N. \tag{4.11}$$

Considering the numerical solution just as a function of Δt, we use the Taylor expansion in that variable and combine (4.8), (4.10), and (4.11) to obtain that

$$\begin{aligned}u_i^{n+1} &= R_i(0,\boldsymbol{u}^n) + \Delta t\frac{\partial R_i(0,\boldsymbol{u}^n)}{\partial \Delta t} + \frac{\Delta t^2}{2}\frac{\partial^2 R_i(0,\boldsymbol{u}^n)}{\partial \Delta t^2} + \mathcal{O}(\Delta t^3) \\ &= u_i^n + \Delta t F_i(\boldsymbol{u}^n) + \frac{\Delta t^2}{2}F_i(\boldsymbol{u}^n)\left[\frac{\partial^2 \varphi_i(0,\boldsymbol{u}^n)}{\partial \Delta t^2} - 2g_i(\boldsymbol{u}^n)\right] + \mathcal{O}(\Delta t^3).\end{aligned} \tag{4.12}$$

Now from (4.2), (4.5), (4.7), and (4.11) we can infer that the difference equation for the error $\boldsymbol{e}^{n+1} := \boldsymbol{u}^{n+1} - \boldsymbol{u}(t^{n+1})$ is

$$\boldsymbol{e}^{n+1} := \boldsymbol{e}^n + \Delta t\begin{pmatrix} F_1(\boldsymbol{u}^n) - F_1(\boldsymbol{u}(t^n)) \\ \vdots \\ F_N(\boldsymbol{u}^n) - F_N(\boldsymbol{u}(t^n))\end{pmatrix} + \frac{\Delta t^2}{2}\begin{pmatrix} \frac{dF_1}{dt}(\boldsymbol{u}^n) - \frac{dF_1}{dt}(\boldsymbol{u}(t^n)) \\ \vdots \\ \frac{dF_N}{dt}(\boldsymbol{u}^n) - \frac{dF_N}{dt}(\boldsymbol{u}(t^n))\end{pmatrix} + \tilde{M}\Delta t^3,$$

for some constant $\tilde{M} > 0$ independent of Δt. Then, if $L = \max\{L_i : 1 \le i \le N\}$ and $\tilde{L} = \max\{\tilde{L}_i : 1 \le i \le N\}$, where L_i and $\tilde{L}_i$, are the Lipschitz constants for F_i and $\partial_t F_i$, respectively. Then for a fixed $j \in \{1,\dots,N\}$, we get the following bound for the local truncation error e_j^{n+1}:

$$\begin{aligned}|e_j^{n+1}| &\le \|\boldsymbol{e}^n\|_\infty + \Delta t\sum_{i=1}^N \big|F_i(\boldsymbol{u}^n) - F_i(\boldsymbol{u}(t^n))\big| + \frac{\Delta t^2}{2}\sum_{i=1}^N \left|\frac{dF_i}{dt}(\boldsymbol{u}^n) - \frac{dF_i}{dt}(\boldsymbol{u}(t^n))\right| + \tilde{M}\Delta t^3 \\ &\le \|\boldsymbol{e}^n\|_\infty + \Delta t\sum_{i=1}^N L_i\big|\boldsymbol{u}^n - \boldsymbol{u}(t^n)\big| + \frac{\Delta t^2}{2}\sum_{i=1}^N \tilde{L}_i\big|\boldsymbol{u}^n - \boldsymbol{u}(t^n)\big| + \tilde{M}\Delta t^3 \\ &\le \left(1 + N\Delta t L + N\frac{\Delta t^2}{2}\tilde{L}\right)\|\boldsymbol{e}^n\|_\infty + \tilde{M}\Delta t^3.\end{aligned}$$

Therefore, we get the following upper bound for the error,

$$\|\boldsymbol{e}^{n+1}\|_\infty \le \left(1 + N\Delta t L + N\frac{\Delta t^2}{2}\tilde{L}\right)\|\boldsymbol{e}^n\|_\infty + \tilde{M}\Delta t^3. \tag{4.13}$$

Then, applying the discrete Gronwall inequality we arrive at

$$\begin{aligned}\|\boldsymbol{e}^n\|_\infty &\le \exp\left(nN\Delta t L + \frac{\Delta t^2}{2} nN\tilde{L}\right)\|\boldsymbol{e}^0\|_\infty + (n\tilde{M}\Delta t^3)\exp\left(nN\Delta t L + \frac{\Delta t^2}{2} nN\tilde{L}\right)\\ &\le \exp\left(NLT + \frac{T^2}{2}N\tilde{L}\right)\|\boldsymbol{e}^0\|_\infty + \exp\left(NLT + \frac{T^2}{2}N\tilde{L}\right)\tilde{M}T\Delta t^2.\end{aligned} \tag{4.14}$$

Hence, we conclude that,

$$\begin{aligned}\|\boldsymbol{u}^n - \boldsymbol{u}(t^n)\|_\infty &\le \exp\left(NLT + \frac{T^2}{2}N\tilde{L}\right)\|\boldsymbol{u}^0 - \boldsymbol{u}(0)\|_\infty + \exp\left(NLT + \frac{T^2}{2}N\tilde{L}\right)T\tilde{M}\Delta t^2\\ &= \mathcal{O}\big(\|\boldsymbol{u}^0 - \boldsymbol{u}(0)\|_\infty\big) + \mathcal{O}(\Delta t^2).\end{aligned} \tag{4.15}$$

Thus, the numerical scheme (2.7) is convergent with order 2. □

Now, if we directly combine the Finite Volume approach described in Section 2.3 to discretize the spatial derivatives while retaining the second-order temporal step (4.1) for the reaction part, the resulting scheme reads as follows: for all $K \in \mathcal{T}$ and $n \in \{0, 1, \dots, M\}$, find $\{u_{i,K}^{n+1}\}_{K\in\mathcal{T}}$ such that

$$m(K)\frac{u_{i,K}^{n+1} - u_{i,K}^n}{\varphi_i\big(\Delta t, \boldsymbol{u}_K^n\big)} - d_i \sum_{L\in\mathcal{N}(K)} \tau_{K|L}(u_{i,L}^{n+1} - u_{i,K}^{n+1}) = m(K)\bar{F}_i(\boldsymbol{u}_K^n, \boldsymbol{u}_K^{n+1}), \quad i = 1, \dots, N. \tag{4.16}$$

We refer to (4.16) as NSFV-1. Although this scheme is dynamically consistent with the reaction system, preserves the positivity of the solutions, and achieves second-order accuracy in space, its temporal accuracy is only first order. This can be established by following the arguments of Theorem 4.1, and is further confirmed numerically in Section 5 through a convergence test. To overcome this limitation, we introduce the so-called Strang splitting technique [57] in the following subsection in order to obtain a new scheme with order 2.

4.2. **Strang-splitting for the diffusion-reaction system.** Having established a second-order NSFD integrator for the reaction subsystem (Theorem 4.1), we now combine it with the finite volume spatial discretization of Section 2.3 into a fully second-order scheme via Strang operator splitting [37]. To start with, we decompose the right-hand side of (1.1) into a reaction operator $\mathcal{R}$ and a diffusion operator $\mathcal{D}$:

$$\mathcal{R}(\boldsymbol{u})_i := F_i(\boldsymbol{u}) = f_i(\boldsymbol{u}) - g_i(\boldsymbol{u})\, u_i, \qquad \mathcal{D}(\boldsymbol{u})_i := d_i\, \Delta u_i, \quad i = 1, \dots, N. \tag{4.17}$$

For component i, the diffusion substep requires advancing the purely diffusive system

$$\frac{d}{dt}V_i(t) = d_i\, \mathcal{L}\, V_i(t), \quad t \in [0, \Delta t], \qquad V_i(0) = U_i^{(1)}, \quad i = 1, \dots, N, \tag{4.18}$$

where $V_i(t) \in \mathbb{R}^{N_e}$ collects the cell-average values over all $K \in \mathcal{T}$, and $\mathcal{L} \in \mathbb{R}^{N_e\times N_e}$ is the finite volume discretization of the Laplacian on the general mesh. The matrix $\mathcal{L}$ is symmetric and negative semi-definite with respect to the discrete inner product $\langle u, v\rangle_\mathcal{T} := \sum_{K\in\mathcal{T}} m(K)\, u_K v_K$. This follows from the discrete integration-by-parts identity

$$-\langle v,\, \mathcal{L}v\rangle_\mathcal{T} = \frac{1}{2}\sum_{K\in\mathcal{T}}\sum_{L\in\mathcal{N}(K)} \tau_{K|L}(v_L - v_K)^2 = |v|_{1,\mathcal{T}}^2 \ge 0, \tag{4.19}$$

where $|\cdot|_{1,\mathcal{T}}$ is the discrete semi-norm defined in (2.10). Given $U^n \approx \boldsymbol{u}(\cdot, t^n)$, the scheme advances one step Δt via the following three sub-steps:

- **Step 1.** We first perform half-step of the reaction part. For each $K \in \mathcal{T}$, compute $U_i^{(1)}$ by applying NSFD-2 scheme described in Algorithm 1 with step size $\Delta t/2$:

$$U_{i,K}^{(1)} = U_{i,K}^n + G_i\big(\tfrac{\Delta t}{2},\, U_K^n\big)\, F_i(U_K^n), \quad i = 1, \dots, N, \tag{4.20}$$

  where

$$G_i(\Delta t, \boldsymbol{u}) := \frac{\varphi_i(\Delta t, \boldsymbol{u})}{1 + \varphi_i(\Delta t, \boldsymbol{u})\, g_i(\boldsymbol{u})}, \tag{4.21}$$

  and $\tau_i(\boldsymbol{u})$ is given by condition (4.2).

- **Step 2.** Next, we perform a full-step in the diffusion part. For each $i = 1, \dots, N$, solve (4.18), i.e. we solve the problem:
$$U_i^{(2)} = \exp(\Delta t d_i \mathcal{L}) U_i^{(1)}. \tag{4.22}$$
- **Step 3.** For each $K \in \mathcal{T}$, repeat Step 1 with step size $\Delta t/2$ and initial data $U^{(2)}$:
$$U_{i,K}^{n+1} = U_{i,K}^{(2)} + G_i\Big(\tfrac{\Delta t}{2}, U_K^{(2)}\Big) F_i(U_K^{(2)}), \quad i = 1, \dots, N. \tag{4.23}$$

We will refer to the scheme (4.20)-(4.23) as NSFV-2 scheme. We notice that the NSFV-2 scheme preserves the positivity of the solution, as stated in the following result.

Theorem 4.2. *Let $U_{i,K}^n \geq 0$ for all $K \in \mathcal{T}$, $i = 1, \dots, N$. Then the solution produced by the NSFV-2 scheme* (4.20)–(4.23) *satisfies $U_{i,K}^{n+1} \geq 0$ for all $K \in \mathcal{T}$, $i = 1, \dots, N$.*

Proof. We verify non-negativity at each substep:

- **Step 1.** Since $f_i \geq 0$, $g_i \geq 0$, $\varphi_i \geq 0$, and $U_{i,K}^n \geq 0$, the update (4.20) satisfies
$$U_{i,K}^{(1)} = \frac{U_{i,K}^n + \varphi_i\big(\frac{\Delta t}{2}, U_K^n\big) f_i(U_K^n)}{1 + \varphi_i\big(\frac{\Delta t}{2}, U_K^n\big) g_i(U_K^n)} \geq 0, \quad \forall\, K \in \mathcal{T},\, i = 1, \dots, N, \tag{4.24}$$
since the numerator and denominator are both non-negative, with the denominator strictly positive.
- **Step 2.** We have from Step 1 that $U_{i,K}^{(1)} \geq 0$, so it is clear that $U_i^{(2)} = \exp(\Delta t d_i \mathcal{L}) U_i^{(1)} \geq 0$, for all $K \in \mathcal{T}$, $i = 1, \dots, N$.
- **Step 3.** From Step 2 we have that $U_{i,K}^{(2)} \geq 0$ and proceeding as in Step 1 we will get that $U_{i,K}^{n+1} \geq 0$, for all $K \in \mathcal{T}$, $i = 1, \dots, N$.

□

The global error of the NSFV-2 scheme receives contributions from two sources. The Strang splitting contributes $O(\Delta t^2)$ globally [37]. It can be shown that, on admissible meshes, the finite volume spatial discretization contributes an error of order $O(h)$ [24]. However, it is well known that finite volume approximations of parabolic problems often exhibit spatial superconvergence. This longstanding phenomenon has recently been addressed for elliptic problems with homogeneous Dirichlet boundary conditions [22], where the authors analyze the superconvergence of a family of gradient schemes, namely the hybrid mimetic mixed (HMM) schemes; estimates for parabolic problems with Neumann boundary conditions are still missing in the finite volume literature. Therefore, since all contributions are expected to be of order 2, the overall accuracy of the NSFV-2 scheme is expected to be $O(\Delta t^2 + h^2)$. This accuracy is confirmed by the numerical experiments presented in Section 5.

5. Numerical examples

The primary aim of this section is to present a set of numerical examples that demonstrate the robustness of the developed schemes. First, we perform a series of convergence tests to show that the developed schemes converge with the expected order. Then, we apply the convergent NSFV scheme to different contexts, where we simulate the behavior of the models in 2D domains with complex geometries. We employ denominator function (4.4) for schemes NSFD-2, NSFV-1, and NSFV-2 in all examples.

5.1. Example 1. Order of accuracy of NSFD-2 schemes.

In this example, we want to check the convergence order of the NSFD-2 method described in Section 4.1. To do so, let us consider a heuristic model with $N = 2$ given by
$$\frac{du_1}{dt} = f_1(u_1, u_2) - u_1 g_1(u_1, u_2), \quad \frac{du_2}{dt} = f_2(u_1, u_2) - u_2 g_2(u_1, u_2),, \tag{5.1}$$

TABLE 1. Example 1. Comparison of $\mathrm{err}_k(T)$ and convergence rate θ_k at simulation time $T = 1$ for different discretizations $M_k = 2^k \cdot 10$ with $k = 0, 1, \ldots, 5$.

		NSFD-1			Euler			NSFD-2			RK-2		
k	M_k	err_k	θ_k	cpu [s]	err_k	θ_k	cpu [s]	err_k	θ_k	cpu [s]	err_k	θ_k	cpu [s]
0	10	6.0e-03	$\star$	4.9e-05	3.0e-04	$\star$	8.7e-05	2.9e-06	$\star$	8.2e-05	4.6e-07	$\star$	1.3e-04
1	20	3.0e-03	0.998	7.0e-05	1.5e-04	1.002	1.1e-04	7.3e-07	1.996	1.3e-04	1.2e-07	2.003	2.2e-04
2	40	1.5e-03	0.999	1.4e-04	7.5e-05	1.001	2.2e-04	1.8e-07	1.998	2.6e-04	2.9e-08	2.001	4.6e-04
3	80	7.5e-04	1.000	2.9e-04	3.8e-05	1.000	4.6e-04	4.6e-08	1.999	5.6e-04	7.2e-09	2.001	9.1e-04
4	160	3.7e-04	1.000	5.7e-04	1.9e-05	1.000	9.2e-04	1.1e-08	2.000	1.1e-03	1.8e-09	2.000	1.9e-03
5	320	1.9e-04	1.000	1.2e-03	9.4e-06	1.000	1.8e-03	2.9e-09	2.000	2.2e-03	4.5e-10	2.000	3.7e-03

with functional responses defined as

$$\begin{aligned} f_1(u_1,u_2) &= \alpha_1 + \frac{\beta_1 u_1^2}{1+u_1^2}, \quad g_1(u_1,u_2) = \gamma_1 + \eta_1 \frac{u_1^2+u_2^2}{1+u_1^2+u_2^2}, \\ f_2(u_1,u_2) &= \alpha_2 + \frac{\beta_2 u_2^2}{1+u_2^2}, \quad g_2(u_1,u_2) = \gamma_2 + \eta_2 \frac{u_1^2+u_2^2}{1+u_1^2+u_2^2}. \end{aligned} \tag{5.2}$$

Let us set the parameters as $\alpha_1 = 0.2, \beta_1 = 0.8, \gamma_1 = 0.5, \eta_1 = 0.3, \alpha_2 = 0.1, \beta_2 = 0.7, \gamma_2 = 0.4, \eta_2 = 0.2$ In this test we set the initial conditions as $u_1^0 = 1.2, u_2^0 = 0.8$. We consider the following sequence of nodes $M_k = 2^k \cdot 10$, which defines a sequence of time-steps $\Delta t_k = T/M_k$, $k = 0, \ldots, 5$. To compare the accuracy of the solutions, we compute a reference solution using a classical fourth-order Runge-Kutta (RK-4) scheme. At each level k, we compute the absolute errors between the solution vector $(u_1^{M_k}, u_2^{M_k})^{\mathrm{T}}$ and the reference solution in the grid of level k, denoted by $(u_{1,\mathrm{ref}}^{M_k}, u_{2,\mathrm{ref}}^{M_k})^{\mathrm{T}}$ i.e. we compute the error at T by using the following expression

$$\mathrm{err}_k(T) := \left|u_1^{M_k} - u_{1,\mathrm{ref}}^{M_k}\right| + \left|u_2^{M_k} - u_{2,\mathrm{ref}}^{M_k}\right|, \quad k = 0, \ldots, 5, \tag{5.3}$$

and the convergence rates were calculated with the following formula

$$\theta_k := \log_2(\mathrm{err}_{k-1}/\mathrm{err}_k), \quad k = 1, \ldots, 5. \tag{5.4}$$

We compare the numerical approximations with respect to the approximations obtained with the NSFD-1 described in Section 2.1 with denominator functions given by $\varphi_i(\Delta t) = \Delta t$, $i = 1, 2$ and the classical first-order Euler scheme and second-order Runge-Kutta scheme (RK-2). In Table 1 we show the approximate error and convergence rate at the simulation time $T = 1$ for different discretizations. Numerical results confirm the second-order accuracy of the NSFD-2 scheme in contrast to the first-order of the Euler and NSFD-1 schemes. In particular, the performance of the NSFD-2 is compared with the Heun scheme (RK2), which can be observed in Figure 5.1. We notice that the NSFD-2 scheme yields slightly larger errors than the Heun method, although the results remain comparable. It should also be noted that the Heun method is slightly more efficient in terms of CPU time, mainly because the NSFD-2 scheme requires additional evaluations at each iteration. Nevertheless, the computational times of both methods are of the same order. In the next Example, however, our numerical method outperforms the Heun scheme.

5.2. **Example 2. Dynamical consistency of the NSFD-2 scheme.** In this example, we aim to illustrate the importance of correctly designing numerical approximations for the reaction terms. To this end, we consider a numerical approximation of the eco-epidemiological system proposed in [53] using the NSFD-2 scheme introduced in Section 4.1. Let X denote the total prey population and Y the predator population. We assume that an infectious disease spreads within the prey population, which is therefore divided into two subpopulations: susceptible individuals, denoted by S, and infected individuals, denoted by I. The

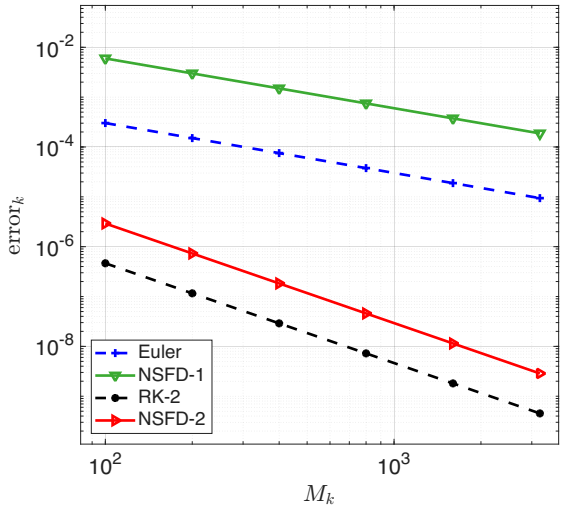

FIGURE 5.1. Example 1. Plot of $\text{err}_k(1)$ against $M_k = 2^k \cdot 10$ with $k = 0, 1, \ldots, 5$, for each scheme tested as a function of M.

governing model equations are given by:

$$\begin{aligned} \frac{dS}{dt} &= rS\left(1 - \frac{S+I}{k}\right) - \lambda SI, \\ \frac{dI}{dt} &= \lambda SI - \frac{\alpha(1-\nu)YI}{a + (1-\nu)I} - \mu I, \\ \frac{dY}{dt} &= Y\left(\delta - \frac{\eta Y}{a + (1-\nu)I}\right), \end{aligned} \tag{5.5}$$

where r is an intrinsic birth rate constant, k is the carrying capacity of the system, λ is the disease transmission coefficient, μ the per capita death rate of infected prey, a is the half saturation constant for infected prey population in absence of refuge, νI is the capacity of a refuge at time t, where $0 < \nu < 1$. This leaves $(1-\nu)I$ of the infected prey available to the predator, and η is the density-dependent mortality of the predator. The endemic equilibrium of this system is given by

$$\mathcal{E}^* = (S^*, I^*, Y^*) = \left(\frac{\alpha(1-\nu)\delta + \eta\mu}{\lambda\eta}, \frac{r\lambda\eta - b(\alpha(1-\nu)\delta + \eta\mu}{\lambda\eta(b+\lambda)}, \frac{\delta}{\eta}\left(a + \frac{b(1-\nu)(\alpha(1-\mu)\delta + \eta\mu)}{\lambda\eta(b+\lambda)}\right)\right),$$

where $b = r/k$. In this example, we demonstrate that the proposed NSFD-2 scheme preserves the stability of this equilibrium, whereas classical schemes such as the forward Euler and RK-2 methods fail to do so for certain values of Δt. To do so, we set the parameters as $r = 5.5, b = 0.3, \lambda = 0.09, \alpha = 1.4, \mu = 0.6, \delta = 0.2, \eta = 0.4, \nu = 0.15, a = 0.2$ and the initial condition as $S^0 = 10, I^0 = 5, Y^0 = 3$. Figure 5.2 displays the numerical solutions of model (5.5) for each component $S(t), I(t)$ and $Y(t)$ for $0 \le t \le 100$, computed with NSFD-2, Euler, and RK-2 schemes for different step sizes $\Delta t \in \{0.1, 0.5, 1\}$. For $\Delta t = 0.1$, we can observe in Figure 5.2 (left column) that all the numerical schemes describe the correct dynamics. However, for $\Delta t \in \{0.5, 1\}$ we can observe in Figure 5.2 (middle and right columns, respectively) some spurious oscillations in the numerical solutions obtained with the Euler and RK-2 schemes. Thus, these results corroborate the unconditional stability of the proposed NSFD-2 numerical scheme for all values of Δt.

5.3. **Example 3. Order of accuracy of NSFV schemes.** For the case of the reaction diffusion system (1.1), we are interested in analyzing both temporal and spatial convergence. To do so, we consider the

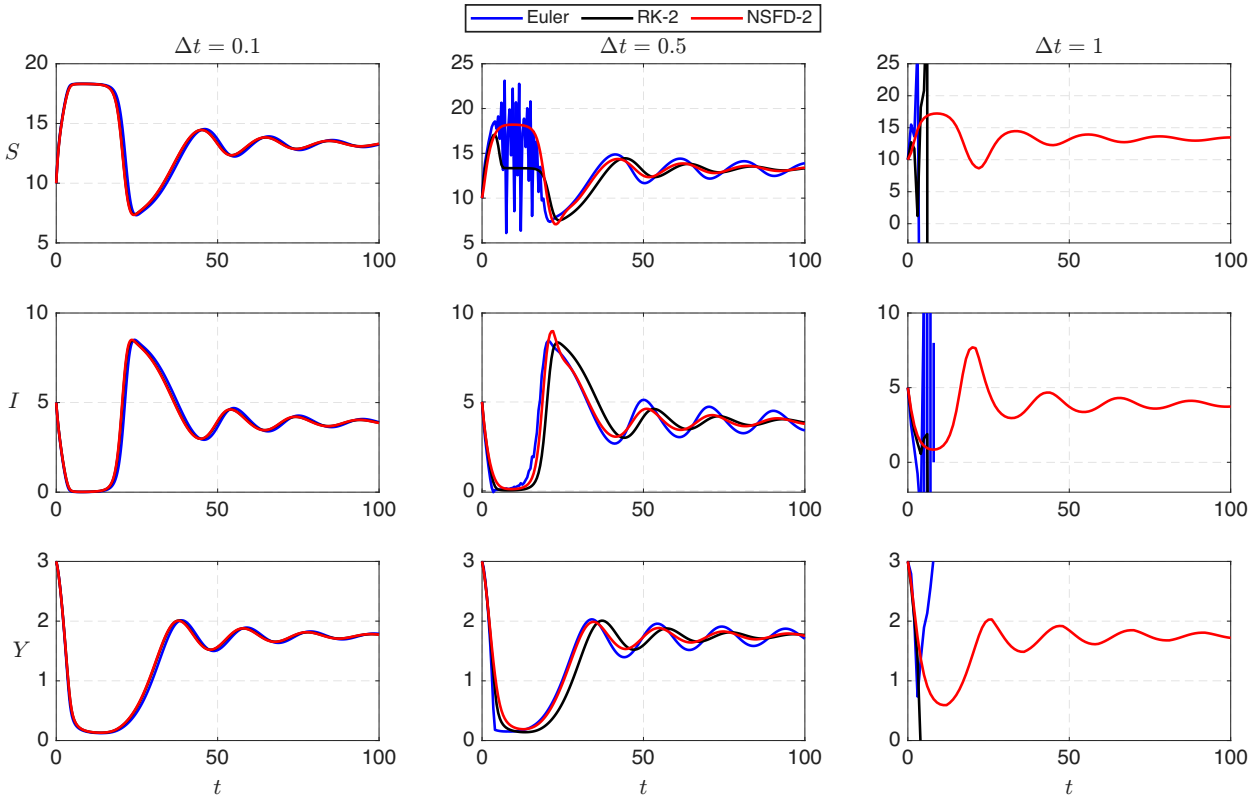

FIGURE 5.2. Example 2. Numerical solutions for the three populations S, I and Y for the ODE model in Example 2, with $0 \leq t \leq 100$ computed with Euler, RK-2 and NSFD-2 numerical schemes with step sizes $\Delta t \in \{0.1, 0.5, 1\}$.

diffusive version of the model studied in Example 1, i.e.

$$\begin{aligned} \frac{\partial u_1}{\partial t} &= d_1 \Delta u_1 + f_1(u_1, u_2) - u_1 g_1(u_1, u_2), \\ \frac{\partial u_2}{\partial t} &= d_2 \Delta u_2 + f_2(u_1, u_2) - u_2 g_1(u_1, u_2), \end{aligned} \tag{5.6}$$

where f_1, f_2, g_1, g_2 are given by (5.2). We posed the model (5.6) in a square domain $\Omega = (0,1) \times (0,1)$ and we consider an structured mesh of $N^x \times N^y$ control volumes given by $\mathcal{T} := \{K_{\ell,j} : \ell = 1, \ldots, N^x, j = 1, \ldots, N^y\}$, where $\Delta x = 1/N^x$, $\Delta y = 1/N^y$, and $K_{\ell,j} := [x_{\ell-1/2}, x_{\ell+1/2}] \times [y_{j-1/2}, y_{j+1/2}]$, $x_{\ell-1/2} := \ell \Delta x$, $\ell = 0, \ldots, N^x$, $y_{j-1/2} := j\Delta y$, $j = 0, \ldots, N^y$. We set the same parameters as in Example 1 and the diffusion coefficients $d_1 = 0.03, d_2 = 0.02$. In addition, we set the initial condition as

$$\begin{aligned} u_1^0(\boldsymbol{x}) &= 1.2 + 0.2\cos(2\pi x)\cos(2\pi y) + 0.1\exp\big(-100\big[(x-0.3)^2 + (y-0.4)^2\big]\big), \\ u_2^0(\boldsymbol{x}) &= 0.8 + 0.1\sin(2\pi x)\sin(2\pi y) + 0.1\exp\big(-120\big[(x-0.7)^2 + (y-0.6)^2\big]\big), \end{aligned}$$

for all $\boldsymbol{x} = (x, y)$ in Ω. Then, we measure the errors as follows: for the temporal order, we chose a fine spatial grid of $N^x \times N^y = 102\,400$ control volumes and a sequence of temporal discretization points $M_k = 5 \cdot 2^k$, for $k = 1, \ldots, 6$. For comparison purposes, we employ a reference solution obtained with the same scheme with $M_{\text{ref}} = 5 \cdot 2^{10}$ points. We measure the errors by components and the total temporal L^∞ error is the measured as:

$$\text{err}_{k,t}^{(i)}(T) := \max_{\substack{1 \leq \ell \leq N^x \\ 1 \leq j \leq N^y}} \left| u_{i,K_{\ell,j}}^{M_k} - u_{i,K_{\ell,j}}^{M_{\text{ref}}} \right|, \quad k = 1, \ldots, 6, \quad i = 1, 2. \tag{5.7}$$

TABLE 2. Example 3. Comparison of $\mathrm{err}_{k,t}^{(i)}(T)$, and convergence rates $\theta_{k,t}^{(i)}$, $i = 1, 2$ at simulation time $T = 1$ for different temporal discretizations $M_k = 2^k \cdot 10$, $k = 0, 1, \ldots, 5$ and for a fixed spatial discretization of $N^x \times N^y = 16384$ control volumes.

		NSFV				NSFV-1				NSFV-2			
k	M_k	$\mathrm{err}_{k,t}^{(1)}$	$\theta_{k,t}^{(1)}$	$\mathrm{err}_{k,t}^{(2)}$	$\theta_{k,t}^{(2)}$	$\mathrm{err}_{k,t}^{(1)}$	$\theta_{k,t}^{(1)}$	$\mathrm{err}_{k,t}^{(2)}$	$\theta_{k,t}^{(2)}$	$\mathrm{err}_{k,t}^{(1)}$	$\theta_{k,t}^{(1)}$	$\mathrm{err}_{k,t}^{(2)}$	$\theta_{k,t}^{(2)}$
0	10	7.6e-03	$\star$	5.2e-03	$\star$	3.0e-03	$\star$	1.9e-03	$\star$	8.3e-05	$\star$	1.0e-04	$\star$
1	20	3.9e-03	0.986	2.6e-03	0.980	1.5e-03	1.001	9.5e-04	1.005	2.1e-05	1.973	2.5e-05	2.066
2	40	1.9e-03	0.995	1.3e-03	0.992	7.4e-04	1.003	4.7e-04	1.005	5.2e-06	2.007	6.0e-06	2.046
3	80	9.6e-04	1.002	6.6e-04	1.000	3.7e-04	1.006	2.3e-04	1.007	1.3e-06	1.989	1.6e-06	1.938
4	160	4.8e-04	1.010	3.3e-04	1.009	1.8e-04	1.012	1.2e-04	1.012	3.3e-07	2.001	3.8e-07	2.048
5	320	2.4e-04	1.022	1.6e-04	1.022	8.9e-05	1.023	5.7e-05	1.023	8.2e-08	1.999	9.5e-08	2.002

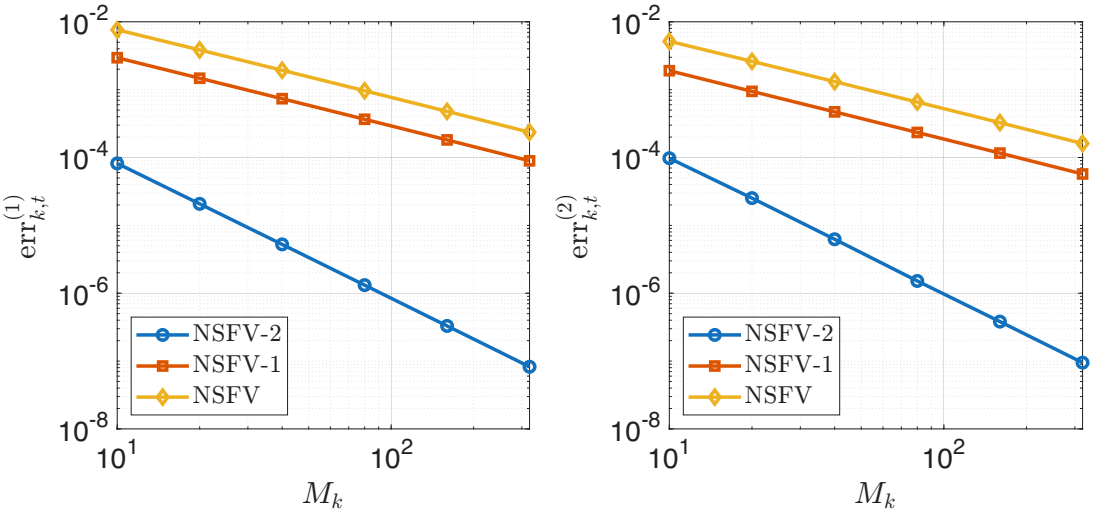

FIGURE 5.3. Example 3: Approximate L^∞ errors for the NSFV, NSFV-1, and NSFV-2 schemes, tested as a function of M, for the (a) first component and (b) second component of the numerical solution.

The convergence rates are computed by the following formula

$$\theta_{k,t}^{(i)} := \log_2 \left(\mathrm{err}_{k-1,t}^{(i)} / \mathrm{err}_{k,t}^{(i)} \right), \quad k = 2, \ldots, 6, \quad i = 1, 2. \tag{5.8}$$

We measure the errors and convergence rates of NSFV, NSFV-1, and NSFV-2 schemes given by (2.13), (4.16), and (4.20)-(4.23), respectively. The approximate L^∞ errors $\mathrm{err}_{k,t}^{(i)}(T)$ defined by (5.7) and their corresponding numerical orders $\theta_{k,t}^{(i)}$ given by (5.8) are displayed in Table 2 at time $T = 1$. The behavior of $\theta_{k,t}^{(i)}$ for increasing values of M confirms first-order convergence in time for schemes NSFV and NSFV-1, and second-order convergence in time for scheme NSFV-2, in each component $i = 1, 2$, which corroborates the discussion in Section 4. We are also interested in studying the spatial convergence rate of the proposed NSFV schemes. To do so, we chose a fine temporal grid of $M = 4000$ points and a sequence of spatial discretization points $N_k^x = N_k^y = 2^k + 1$, for $k = 2, \ldots, 6$. For comparison purposes, we employ a reference solution obtained with the same scheme with $N_{\mathrm{ref}}^x \times N_{\mathrm{ref}}^y = 66049$ control volumes. We then measure the L^1

TABLE 3. Example 3. Comparison of $\mathrm{err}^{(i)}_{k,\boldsymbol{x}}(T)$, and convergence rates $\theta^{(i)}_{k,\boldsymbol{x}}$, $i = 1, 2$ at simulation time $T = 1$ for different spatial discretizations $N^x_k = N^y_k = 2^k + 1$, $k = 2, \dots, 6$ and for a fixed temporal discretization of $M = 4000$ temporal steps.

		NSFV				NSFV-1				NSFV-2			
k	$N^x_k \times N^y_k$	$\mathrm{err}^{(1)}_{k,\boldsymbol{x}}$	$\theta^{(1)}_{k,\boldsymbol{x}}$	$\mathrm{err}^{(2)}_{k,\boldsymbol{x}}$	$\theta^{(2)}_{k,\boldsymbol{x}}$	$\mathrm{err}^{(1)}_{k,\boldsymbol{x}}$	$\theta^{(1)}_{k,\boldsymbol{x}}$	$\mathrm{err}^{(2)}_{k,\boldsymbol{x}}$	$\theta^{(2)}_{k,\boldsymbol{x}}$	$\mathrm{err}^{(1)}_{k,\boldsymbol{x}}$	$\theta^{(1)}_{k,\boldsymbol{x}}$	$\mathrm{err}^{(2)}_{k,\boldsymbol{x}}$	$\theta^{(2)}_{k,\boldsymbol{x}}$
2	25	2.2e-03	$\star$	3.9e-03	$\star$	3.0e-03	$\star$	3.9e-03	$\star$	2.2e-03	$\star$	3.9e-03	$\star$
3	81	5.5e-04	2.034	9.0e-04	2.129	5.5e-04	2.034	9.0e-04	2.129	5.5e-04	2.034	9.0e-04	2.129
4	289	1.4e-04	2.017	2.2e-04	2.048	1.4e-04	2.017	2.2e-04	2.048	1.4e-04	2.017	2.2e-04	2.048
5	1089	3.3e-05	2.029	5.3e-05	2.025	3.3e-05	2.029	5.3e-05	2.025	3.3e-05	2.029	5.3e-05	2.025
6	4225	7.9e-06	2.074	1.3e-05	2.073	7.9e-06	2.074	1.3e-05	2.073	7.9e-06	2.074	1.3e-05	2.073

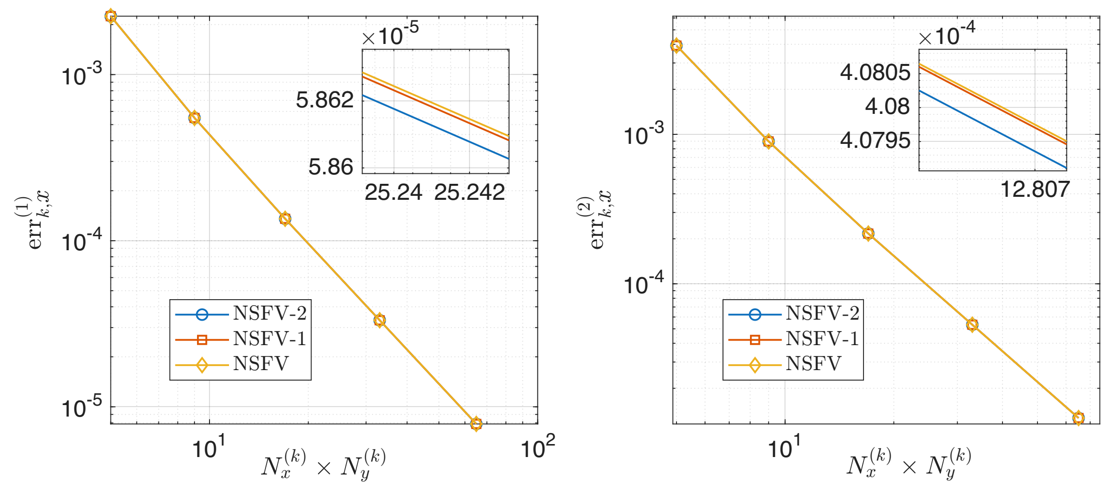

FIGURE 5.4. Example 3: Approximate spatial L^1 errors for the NSFV, NSFV-1, and NSFV-2 schemes, tested as a function of $N^x \times N^y$, for the (a) first component and (b) second component of the numerical solution.

errors by components as:

$$\mathrm{err}^{(i)}_{k,\boldsymbol{x}}(T) := \Delta x \Delta y \sum_{\ell=1}^{N^x_k} \sum_{j=1}^{N^y_k} \left| \tilde{u}^M_{i,K_{\ell,j}}(T) - u^M_{i,K_{\ell,j}}(T) \right|, \quad k = 1, \dots, 5, \quad i = 1, 2, \tag{5.9}$$

where $\tilde{u}^M_{i,K_{\ell,j}}$ is the projection of the reference solution in the coarse k-th grid. The convergence rates are calculated with the following formula

$$\theta^{(i)}_{k,\boldsymbol{x}} := \log_2 \left(\mathrm{err}^{(i)}_{k-1,\boldsymbol{x}} / \mathrm{err}^{(i)}_{k,\boldsymbol{x}} \right), \quad k = 2, \dots, 6, \quad i = 1, 2. \tag{5.10}$$

The results for this test are displayed in Table 3. The behavior of $\theta^{(i)}_{k,\boldsymbol{x}}$ for increasing values of $N^x \times N^y$ confirms second-order convergence in space for all schemes NSFV, NSFV-1, and NSFV-2, in each component $i = 1, 2$, which corroborates the discussion made at the end of Section 4.

5.4. **Example 4. Applications of the numerical scheme.** The following numerical experiments are designed to illustrate the versatility of the proposed convergent NSFV numerical method. We consider numerical simulations arising in epidemiological and ecological contexts, showing that the scheme accurately describes the epidemic. In addition, simulations show that the scheme is capable of capturing Turing patterns

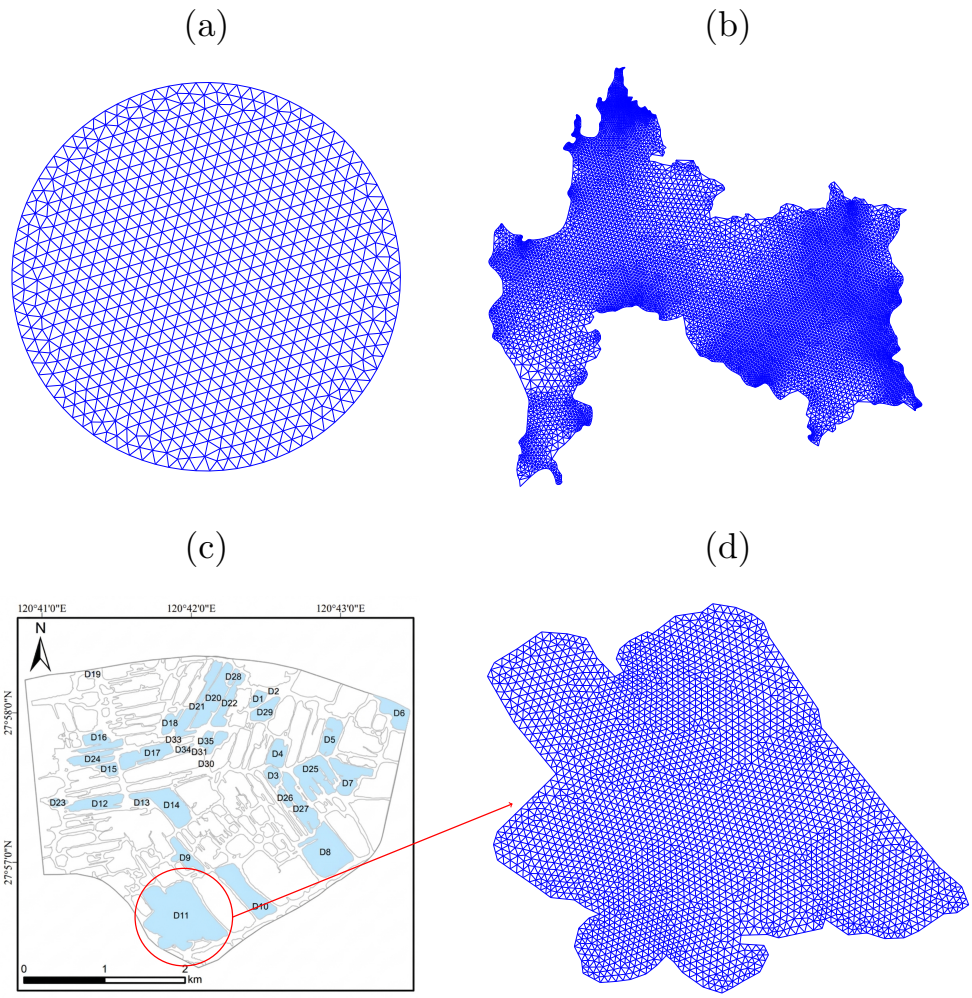

FIGURE 5.5. (a) Circular domain of Example 5.4.2 and reference mesh with 1499 triangles. (b) Mesh of the Biobío region in Chile used in Example 5.4.1 with 18098 triangles. (c) Map of the Sanyang Wetland in Wenzhou City, Zhejiang Province, China taken from [38], and (d) a reference triangulation of the D11 sector used in Example 5.4.3 with 5430 triangles.

predicted by theoretical analysis in ecological contexts [25, 58]. Moreover, the numerical experiments are performed on complex geometries, thereby demonstrating that the method is not restricted to rectangular computational domains. This is one main advantage of numerical schemes based on finite volumes.

5.4.1. *Application to a SIR model.* Mathematical models that describe the spread of a disease based on PDEs have been proposed in [9, 27, 42]. If S, I, and R represent the numbers of susceptible, infected, and recovered individuals, respectively, a diffusive SIR epidemic model can be formulated as follows:

$$\begin{aligned}
\frac{\partial S}{\partial t} &= d_S \Delta S + \Lambda - \frac{\beta S I}{1+\alpha I} - \mu S, \\
\frac{\partial I}{\partial t} &= d_I \Delta I + \frac{\beta S I}{1+\alpha I} - \frac{\gamma I}{1+\alpha I} - (\mu + d + \gamma) I, \\
\frac{\partial R}{\partial t} &= d_R \Delta R + \delta I + \frac{\gamma I}{1+\alpha I} - \mu R,
\end{aligned} \tag{5.11}$$

where Λ denotes the inflow population (newborns and immigration), μ is the natural death rate, d is the disease-induced death rate, γ is the natural recovery rate, and d_S, d_I, and d_R denote the diffusion rates of susceptible, infected, and recovered individuals, respectively. In this model, the infection occurs at a nonlinear saturated incidence rate defined as $\frac{\beta SI}{1+\alpha I}$, where $\beta > 0$ denotes the transmission or contact rate, while $\alpha > 0$ is a saturation parameter that reflects behavioral responses or constraints on contact opportunities when the infected population becomes large. In addition, the treatment process is modeled by the term $\frac{\gamma I}{1+\alpha I}$, where γ denotes the maximum per capita treatment rate, and α is a saturation parameter that accounts for treatment delays caused by limited healthcare resources or congestion. Notice that (5.11) can be put in the form of (1.1), with response functions f_i and g_i defined by

$$\begin{aligned} f_S(S,I,R) &= \Lambda, \quad g_S(S,I,R) = \frac{\beta I}{1+\alpha I} + \mu, \\ f_I(S,I,R) &= \frac{\beta SI}{1+\alpha I}, \quad g_I(S,I,R) = \frac{\gamma}{1+\alpha I} + \mu + d + \gamma, \\ f_R(S,I,R) &= \delta I + \frac{\gamma I}{1+\alpha I}, \quad g_R(S,I,R) = \mu, \end{aligned} \tag{5.12}$$

which satisfy assumptions (1.2) in $\Sigma = \mathbb{R}^N_+$. According to Theorem 3.4 in [64], model (5.11) admits the same basic reproduction number as its ODE counterpart. Employing the next-generation matrix technique [61] one can show that $\mathcal{R}_0 = \frac{\beta\Lambda}{\mu(\mu+d+\delta+\gamma)}$. To illustrate the ability of the NSFV-1 scheme (2.13) to accurately describe epidemic dynamics, we consider a spatial domain shaped like the Biobío Region in Chile. We take parameters as $\Lambda = 1$, $\beta = 2.4$, $\alpha = 0.5$, $\mu = 0.2$, $\gamma = 0.3$, $\delta = 0.25$, $d = 0.05$, $d_S = 0.05$, $d_I = 0.002$, $d_R = 0.03$. Let $\beta_{\text{crit}} > 0$ be such that $\mathcal{R}_0 = 1$, i.e. $\beta_{\text{crit}} = \frac{\mu(\mu+d+\delta+\gamma)}{\Lambda}$, so the spread of the infection is analyzed in two scenarios. In Scenario 1, we consider $\beta_* = 1.2\beta_{\text{crit}}$, so $\mathcal{R}_0 > 1$; and in Scenario 2, we choose $\beta^* = 0.9\beta_{\text{crit}}$ so that $\mathcal{R}_0 < 1$. We fix an initial infection hotspot located at (x_0, y_0) in the capital city, Concepción (see Figure 5.6), i.e. we set:

$$S^0(\boldsymbol{x}) = \Lambda/\mu, \quad I^0(\boldsymbol{x}) = 0.25\exp\left(\frac{-(x-x_0)^2-(y-y_0)^2}{2\sigma^2}\right), \quad R^0(\boldsymbol{x}) = 0, \quad \boldsymbol{x} \in \Omega,$$

for $\boldsymbol{x} = (x, y)$ in Ω and $\sigma = 0.5203$. We simulate system (5.11) until $t = 30$ and using a time step size $\Delta t = 0.5$. As shown in Figure 5.6, the scheme successfully reproduces the expected qualitative behavior of the solutions. In particular, the infection spreads when $\mathcal{R}_0 > 1$ (Scenario 1), whereas the disease eventually dies out when $\mathcal{R}_0 < 1$ (Scenario 2).

5.4.2. *Application to a food chain model.* In [68] the authors proposed a diffusive food chain model describing the interaction between a prey, an intermediate predator, and a top predator, i.e., a predator of the whole ecosystem. If u stands for the prey density, w is the top predator density, and v describes the density of the intermediate predator. Thus, the equations for the mathematical model are as follows

$$\begin{aligned} \frac{\partial u}{\partial t} &= d_1\Delta u + u(1-u) - \frac{c_1 uv}{u+v}, \\ \frac{\partial v}{\partial t} &= d_2\Delta v + \frac{m_1 uv}{u+v} - q_1 v - \frac{c_2 vw}{v+w}, \\ \frac{\partial w}{\partial t} &= d_3\Delta w + \frac{m_2 vw}{v+w} - q_2 w, \end{aligned} \tag{5.13}$$

where c_1 and c_2 are the maximum ingestion rates of intermediate predator and top predator, m_1 is the conversion factor of prey to intermediate predator, m_2 is the conversion factor of intermediate predator, q_1 is the food-independent death rate of the intermediate predator, and q_2 is the food-independent death rate of the top predator, and d_1, d_2, and d_3 are the diffusion coefficients of the three species. In this case, the

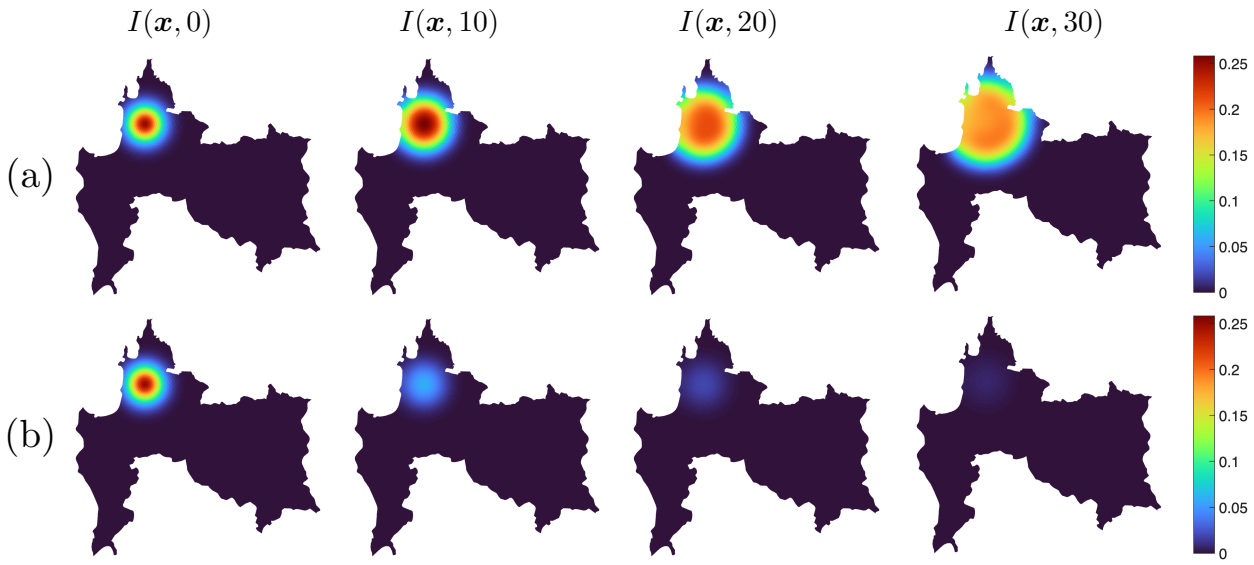

FIGURE 5.6. Spread of the infection in two cases (a) Scenario 1, where the basic reproduction number satisfies $\mathcal{R}_0 > 1$ and (b) Scenario 2, where the basic reproduction number satisfies $\mathcal{R}_0 < 1$.

response functions f_i and g_i are given by

$$\begin{aligned} f_1(u,v,w) &= u, & g_1(u,v,w) &= u + \frac{c_1 v}{u+v}, \\ f_2(u,v,w) &= \frac{m_1 uv}{u+v}, & g_2(u,v,w) &= q_1 + \frac{c_2 w}{v+w}, \\ f_3(u,v,w) &= \frac{m_2 vw}{v+w}, & g_3(u,v,w) &= q_2. \end{aligned} \tag{5.14}$$

Notice that functions (5.14) satisfy hypothesis (1.2) in the admissible rectangle $\Sigma = \{(u,v,w) : 0 < u \leq 1,\ v > 0,\ w > 0\}$. Provided that the initial condition $\boldsymbol{u}^0$ belongs to Σ, we can follow Lemma 3.2 in [11] to show that the NSFV scheme (2.13) preserves this invariant rectangle. The goal of this test is to reproduce the Turing pattern formation analyzed in [68] for different values of the parameters in a complex geometry. In this case, we define the mathematical model in a circle-shaped domain. We discretize the domain with a triangulation $\mathcal{T} = \{K_j : j = 1, \ldots, N_e\}$, with $N_e = 23438$ triangles (see Figure 5.5 (a) for a reference mesh of Ω) and set $\Delta t = 1$. We set the parameters $m_1 = 1.5$, $m_2 = 2$, $q_1 = 0.6$, $q_2 = 1$, $c_2 = 0.5$, $d_1 = 0.01$, $d_2 = 0.1$, $d_3 = 1$. We vary the parameters (q_1, c_1) in order to obtain the same patterns as in [68] in our circle-shaped domain. The initial condition is set to be a perturbation of the interior equilibrium point $\mathcal{E}^* = (u^*, v^*, w^*) = (0.20267, 0.15498, 0.15498)$, i.e.

$$z^0(\boldsymbol{x}) = \sum_{j=1}^{N_e} (z^* + \mathrm{per}_j)\chi_{K_j}(\boldsymbol{x}), \quad \boldsymbol{x} \in \Omega, \quad z \in \{u, v, w\}, \tag{5.15}$$

where $\mathrm{per}_j = (2\xi_j - 1) \cdot (5 \times 10^{-4})$, and $\xi_j \sim \mathcal{U}(0,1)$, i.i.d. for $j = 1, \ldots, N_e$. We then investigate the influence of the parameter c_1 by considering different values of it and recovering some of the pattern formations described in [68]. These results are shown in Figure 5.7. For $c_1 = 1.84$, the model displays a regular pattern of holes. As c_1 is increased to 1.95, the dynamics undergo a transition from stripe-hole growth to stripe replication; in other words, the holes gradually disappear and a stripe pattern develops. Finally, for $c_1 = 2.21$, a spot pattern is formed. Furthermore, we observe that higher values of the parameter c_1 lead to smaller prey densities. This is due to a larger predator effect on the prey in the ratio-dependent

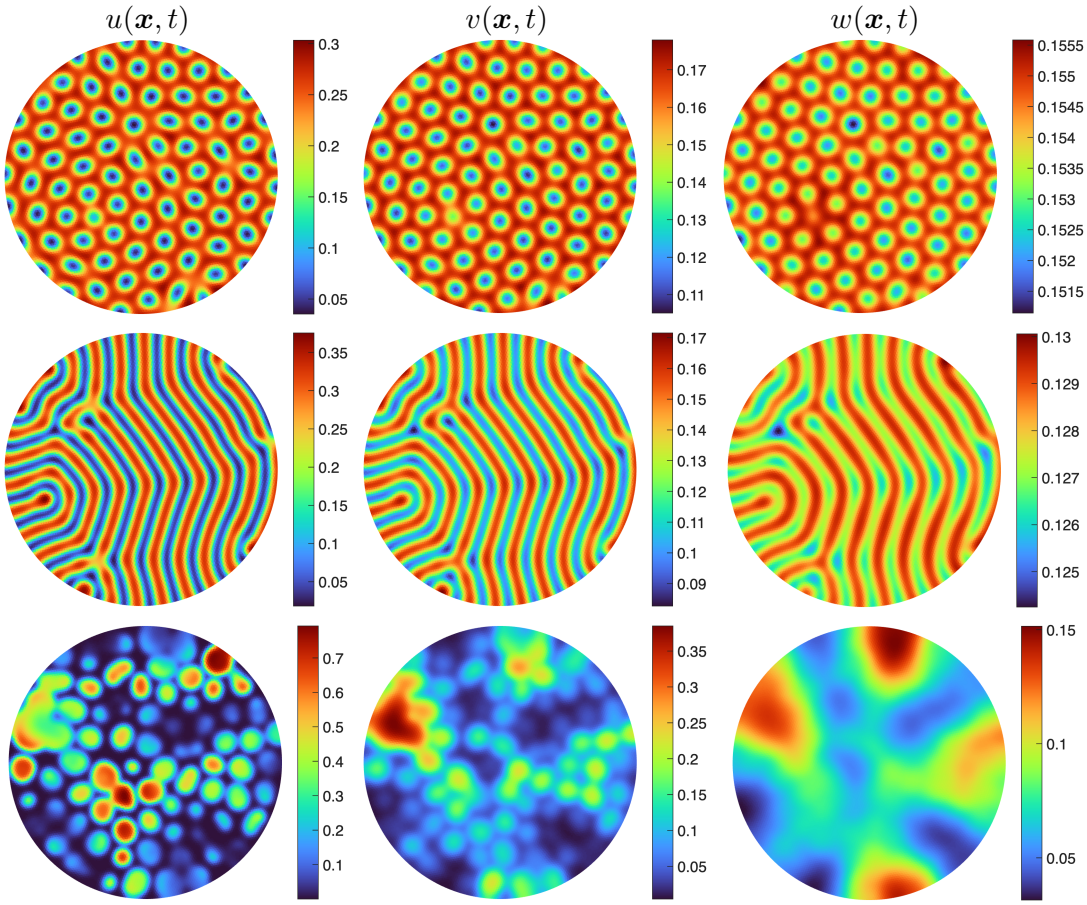

FIGURE 5.7. Numerical solutions of the concentrations $u(\boldsymbol{x},t)$, $v(\boldsymbol{x},t)$, and $w(\boldsymbol{x},t)$ at $t = 20000$ for $c_1 = 1.84$ (first row), at $t = 20000$ for $c_1 = 1.95$ (second row), and at $t = 100000$ for $c_1 = 2.21$ (third row) in Example 5.4.2.

functional response. The increase in c_1 describes a faster consumption of the prey by the predator since the parameter c_1 represents the maximum per capita grazing or attack rate of the predator v on u.

5.4.3. *Application to a nutrient-algae model.* In this numerical simulation, we consider the model studied in [65,66] that describes a diffusive nutrient-algae model based on the Sanyang Wetland located in Wenzhou, China. Let u and v denote the nutrient concentration and the algae density in the wetland, respectively. The equations describing the dynamics of the ecosystem are given by [65]:

$$\begin{aligned} \frac{\partial u}{\partial t} &= d_1 \Delta u + I - bu + \frac{u^2}{1+u^2} - auv, \\ \frac{\partial v}{\partial t} &= d_2 \Delta v + rv\left(1 - \frac{v}{k}\right) + aeuv - mv, \end{aligned} \tag{5.16}$$

where I is the input rate of nutrients flowing into the water, a is the maximum growth rate of the algae population, e is the efficiency of conversion, r is the intrinsic growth rate, k the carrying capacity of the algae population, m the death rate of the algae population, and d_1 and d_2 are the diffusion coefficients of

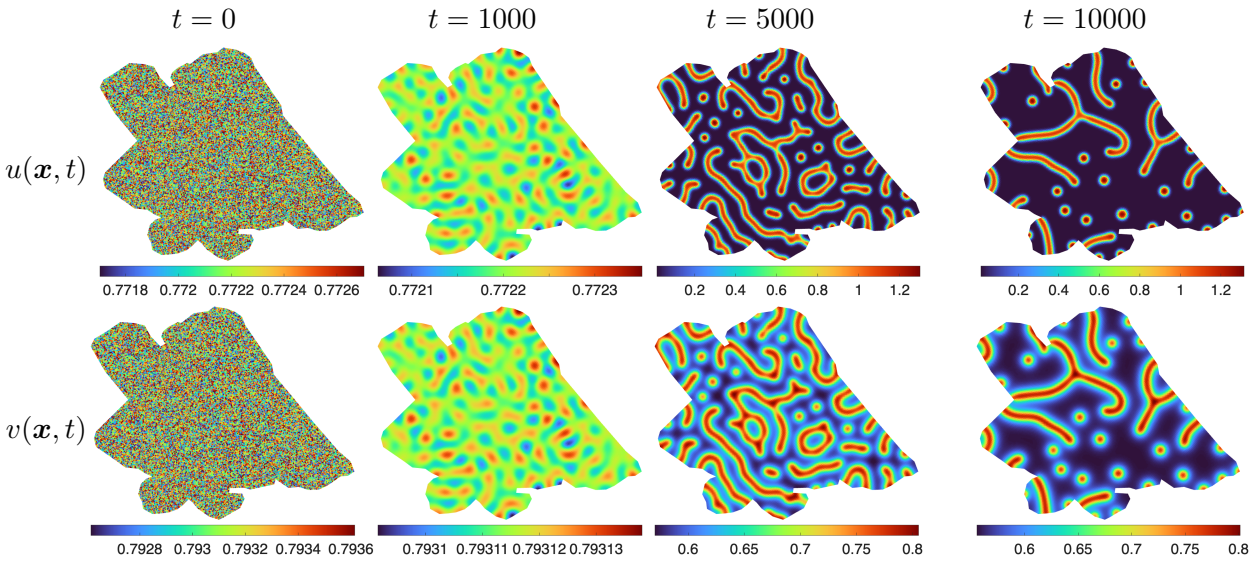

FIGURE 5.8. Numerical solutions of the concentrations of nutrients $u(\boldsymbol{x}, t)$ (first row) and algae density $v(\boldsymbol{x}, t)$ (second row) for model (5.16) over the time interval $0 \leq t \leq 10000$. Snapshots are shown at $t = 0$ (initial condition), $t = 1000$, $t = 5000$, and $t = 10000$.

nutrients and algae, respectively. In this case the response functions f_i and g_i are given by

$$\begin{aligned} f_1(u, v) &= I + \frac{u^2}{1 + u^2}, \qquad g_1(u, v) = b + av, \\ f_2(u, v) &= rv + aeuv, \qquad g_2(u, v) = \frac{r}{k}v + m. \end{aligned} \tag{5.17}$$

Notice that functions (5.17) satisfy hypothesis (1.2) in the admissible rectangle $\Sigma = \{(u, v) : 0 \leq u,\ 0 \leq v \leq 1\}$. To study the Turing pattern formation, we set the parameters $I = 0.0055, a = 0.6, b = 0.015, e = 0.28, r = 0.533, k = 1, m = 0.24, d_1 = 0.1, d_2 = 1.4$. The initial condition is set to be a perturbation of the interior equilibrium point $\mathcal{E}^* = (u^*, v^*) = (0.77220, 0.79311)$, i.e. u^0 and v^0 is defined as in (5.15). We simulate until $t = 10000$ with a time step of $\Delta t = 10$. Notice that this is a relatively large time step size. Despite this the numerical simulations generated with our proposed NSFV scheme reproduce the Turing pattern formation. In Figure 5.8, we present snapshots at different times illustrating that the NSFV scheme correctly captures the Turing pattern formation reported in [65] on a complex geometrical domain representing the geography of the ecosystem under study.

6. CONCLUSIONS

In this work, we proposed and analyzed a finite volume scheme for a diffusion-production-destruction model where the functions appearing in the reaction part satisfies certain general assumptions. The first contribution of this work is the presentation of a novel FV scheme that combines a standard finite volume discretization of the spatial operators with a nonstandard finite difference (NSFD) approach for the reaction terms. This proposed FV scheme ensures that the discrete dynamics reproduce the qualitative behavior of the spatially homogeneous system, as described in Section 2.1. In addition, we prove the existence of the discrete solution of the resulting scheme. The second contribution is the proof of convergence of the scheme. We employed L^2-estimates and compactness arguments to establish that a sequence of discrete solutions generated by this scheme converges to an admissible weak solution of the model, as stated in Theorem 3.6. In Section 4, we proposed a second-order extension in both space and time that preserves positivity. We first employed a second-order NSFD discretization for the reaction operator and observed that the direct combination of this discretization with a standard FV discretization of the Laplacian yields a scheme that is

second-order in space but only first-order in time. To overcome this limitation, we combined the second-order NSFD scheme for the reaction part with a Strang splitting approach for the spatial approximation.
In Section 5, through a series of numerical experiments, we demonstrate that all proposed schemes converge with the optimal order of accuracy predicted by the theory. Furthermore, we show that the NSFV scheme exhibits robustness with respect to the domain geometry, the time-step size, and variations in the model parameters. In addition, the scheme is shown to reproduce the different kinds of Turing patterns previously reported for different models in ecology, demonstrating that the discretization is not only stable but also capable of capturing complex spatial morphologies.
Finally, we are interested in developing arbitrarily high-order versions of the proposed scheme that preserve key qualitative properties of the continuous model, such as the positivity and boundedness of the solutions, as well as dynamical consistency with the corresponding ODE model. Furthermore, we aim to explore the applicability of these schemes to models with heterogeneous coefficients and time delays arising in the description of epidemic dynamics in complex scenarios.

Acknowledgments. Abraham J. Arenas is supported by Universidad de Córdoba (sabbatical year) and for Vicerrectoría de Investigación y Extensión of Universidad de Córdoba. Juan Barajas-Calonge is supported by the National Agency for Research and Development, ANID-Chile through the Scholarship Program, Becas Doctorado Nacional 2022, 21221387. Luis Miguel Villada is supported by ANID - Chile through of Centro de Modelamiento Matemático (CMM), project FB210005 of BASAL funds for Centers of Excellence. This paper is part of the Juan Barajas-Calonge Ph.D. thesis in the Program Doctorado en Matemática Aplicada, Universidad del Bío-Bío.

References

[1] M. Abbas, F. Giannino, A. Iuorio, Z. Ahmad, and F. Calabró, *PDE models for vegetation biomass and autotoxicity*, Mathematics and Computers in Simulation, 228 (2025), pp. 386–401.
[2] A. A. Aderogba, M. Chapwanya, J. Djoko Kamdem, and J.-S. Lubuma, *Coupling finite volume and nonstandard finite difference schemes for a singularly perturbed Schrödinger equation*, International Journal of Computer Mathematics, 93 (2016), pp. 1833–1844.
[3] N. Ahmed, A. Elsonbaty, A. Raza, M. Rafiq, and W. Adel, *Numerical simulation and stability analysis of a novel reaction–diffusion COVID-19 model*, Nonlinear Dynamics, 106 (2021), pp. 1293–1310.
[4] M. A. Ali, H. J. Eberl, and R. Sudarsan, *Numerical solution of a degenerate, diffusion-reaction based biofilm growth model on structured non-orthogonal grids*, Commun. Comput. Phys, 24 (2018), pp. 695–741.
[5] B. Andreianov, M. Bendahmane, and M. Saad, *Finite volume methods for degenerate chemotaxis model*, Journal of computational and applied mathematics, 235 (2011), pp. 4015–4031.
[6] A. Appadu, G. de Waal, and C. Pretorius, *Nonstandard finite difference methods for a convective predator-prey pursuit and evasion model*, Journal of Difference Equations and Applications, 30 (2024), pp. 1808–1841.
[7] A. R. Appadu, J. K. Djoko, H. Gidey, and J. M.-S. Lubuma, *Analysis of multilevel finite volume approximation of 2D convective Cahn–Hilliard equation*, Japan Journal of Industrial and Applied Mathematics, 34 (2017), pp. 253–304.
[8] A. J. Arenas, G. González-Parra, and B. M. Caraballo, *A nonstandard finite difference scheme for a nonlinear Black–Scholes equation*, Mathematical and Computer Modelling, 57 (2013), pp. 1663–1670.
[9] E. Avila-Vales, G. E. Garcia-Almeida, and A. G. Perez, *Qualitative analysis of a diffusive SIR epidemic model with saturated incidence rate in a heterogeneous environment*, Journal of Mathematical Analysis and Applications, 503 (2021), p. 125295.
[10] H. Banda, M. Chapwanya, and P. Dumani, *Pattern formation in the Holling–Tanner predator–prey model with predator-taxis. a nonstandard finite difference approach*, Mathematics and Computers in Simulation, 196 (2022), pp. 336–353.
[11] J. Barajas-Calonge, M. Sepulveda, N. Torres, and L. M. Villada, *Dynamically consistent finite volume scheme for a bimonomeric simplified model with inflammation processes for Alzheimer's disease*, arXiv preprint arXiv:2512.10716, (2025).
[12] M. Bendahmane, Z. Khalil, and M. Saad, *Convergence of a finite volume scheme for gas-water flow in a multi-dimensional porous medium*, Mathematical Models and Methods in Applied Sciences, 24 (2014), pp. 145–185.
[13] A. Berman and R. J. Plemmons, *Nonnegative matrices in the mathematical sciences*, SIAM, 1994.
[14] A. L. Bertozzi, N. Drenska, J. Latz, and M. Thorpe, *Partial differential equations in data science*, Philosophical transactions. Series A, Mathematical, physical, and engineering sciences, 383 (2025), p. 20240249.
[15] C. Chainais-Hillairet, J.-G. Liu, and Y.-J. Peng, *Finite volume scheme for multi-dimensional drift-diffusion equations and convergence analysis*, ESAIM: Mathematical Modelling and Numerical Analysis, 37 (2003), pp. 319–338.
[16] M. Choiński, *A non–standard discretized SIS model of co–infection in a heterogeneous population*, Journal of Difference Equations and Applications, (2026), pp. 1–27.

[17] P. Colli, G. Marinoschi, E. Rocca, and A. Viguerie, *Chemotaxis-inspired PDE model for airborne infectious disease transmission: analysis and simulations*, Journal of Nonlinear Science, 35 (2025), p. 28.
[18] D. Conte, G. Pagano, and B. Paternoster, *Nonstandard finite differences numerical methods for a vegetation reaction–diffusion model*, Journal of Computational and Applied Mathematics, 419 (2023), p. 114790.
[19] Y. Coudière, M. Saad, and A. Uzureau, *Analysis of a finite volume method for a bone growth system in vivo*, Computers & Mathematics with Applications, 66 (2013), pp. 1581–1594.
[20] J. Cresson and F. Pierret, *Non standard finite difference scheme preserving dynamical properties*, Journal of Computational and Applied mathematics, 303 (2016), pp. 15–30.
[21] A. Daher, D. Trucu, and R. Eftimie, *Calibrating tissue level PDE models of ligand dynamics using single cell and spatial transcriptomics data*, npj Systems Biology and Applications, (2026).
[22] J. Droniou and N. Nataraj, *Improved estimate for gradient schemes and super-convergence of the TPFA finite volume scheme*, IMA Journal of Numerical Analysis, 38 (2018), pp. 1254–1293.
[23] M. Ehrhardt and A. Gumel, *Nonstandard finite difference schemes for the Black–Scholes equation*, Mathematics of Continuous and Discrete Dynamical Systems: Contemporary Mathematics, 618 (2014), p. 217.
[24] R. Eymard, T. Gallouët, and R. Herbin, *Finite volume methods*, in Solution of Equation in $\mathbb{R}^n$ (Part 3), Techniques of Scientific Computing (Part 3), vol. 7 of Handbook of Numerical Analysis, Elsevier, 2000, pp. 713–1018.
[25] J. D. Ferreira, L. M. Echeverry, and C. A. P. Rincon, *Stability and bifurcation in epidemic models describing the transmission of toxoplasmosis in human and cat populations*, Mathematical Methods in the Applied Sciences, 40 (2017), pp. 5575–5592.
[26] E. Friedmann, *PDE/ODE modeling and simulation to determine the role of diffusion in long-term and-range cellular signaling*, BMC biophysics, 8 (2015), p. 10.
[27] G. González-Parra, C.-L. Pérez, M. Llamazares, R.-J. Villanueva, and J. Villegas-Villanueva, *Challenges in the mathematical modeling of the spatial diffusion of SARS-CoV-2 in Chile*, Mathematical biosciences and engineering: MBE, 22 (2025), p. 1680.
[28] J. Guo, H. Zhu, Y. Yang, and C. Guo, *Advances in physics-informed neural networks for solving complex partial differential equations and their engineering applications: A systematic review*, Engineering Applications of Artificial Intelligence, 161 (2025), p. 112044.
[29] D. Gutierrez-Oribio, Y. Orlov, I. Stefanou, and F. Plestan, *Robust boundary tracking control of wave PDE: Insight on forcing slow-aseismic response*, Systems & Control Letters, 178 (2023), p. 105571.
[30] L. Heimbach, S. Kaltenbach, P. Karnakov, F. J. Alexander, and P. Koumoutsakos, *Reinforcement learning closures for underresolved partial differential equations using synthetic data*, Computer Methods in Applied Mechanics and Engineering, 452 (2026), p. 118767.
[31] M. T. Hoang, *High-order nonstandard finite difference methods preserving dynamical properties of one-dimensional dynamical systems*, Numerical Algorithms, 98 (2025), pp. 219–249.
[32] M. T. Hoang and M. Ehrhardt, *A second-order nonstandard finite difference method for a general Rosenzweig–MacArthur predator–prey model*, Journal of Computational and Applied Mathematics, 444 (2024), p. 115752.
[33] ———, *Differential equation models for infectious diseases: Mathematical modeling, qualitative analysis, numerical methods and applications: Mt hoang, m. ehrhardt*, SeMA Journal, (2025), pp. 1–36.
[34] M. T. Hoang and M. Ehrhardt, *A generalized second-order positivity-preserving numerical method for non-autonomous dynamical systems with applications*, Applied Mathematics and Computation, 524 (2026), p. 130029.
[35] A. Jourdon and D. A. May, *An efficient partial-differential-equation-based method to compute pressure boundary conditions in regional geodynamic models*, Solid Earth, 13 (2022), pp. 1107–1125.
[36] S. Kopecz and A. Meister, *A comparison of numerical methods for conservative and positive advection-diffusion-production-destruction systems*, PAMM, 19 (2019), p. e201900209.
[37] C. Liu, C. Wang, and Y. Wang, *A second-order accurate, operator splitting scheme for reaction-diffusion systems in an energetic variational formulation*, SIAM Journal on Scientific Computing, 44 (2022), pp. A2276–A2301.
[38] J. Liu, M. Chen, L. Wang, T. Liu, X. Jin, F.-H. Yu, and Y. Zhang, *Habitat fragmentation differentially affects invasive and native plant diversity in a human-dominated wetland island system*, Plant Diversity, (2024).
[39] W. Magrogan, N. Rodríguez, and J. Brantingham, *Reaction–diffusion dynamics of protesting activity on networks: spreading speeds, Allee effects, and wave pinning*, Bollettino dell'Unione Matematica Italiana, (2026), pp. 1–26.
[40] R. Mickens and T. Washington, *A note on a NSFD discretization of a sobolev type PDE*, Journal of Difference Equations and Applications, 31 (2025), pp. 292–297.
[41] R. E. Mickens, *Nonstandard finite difference models of differential equations*, World Scientific, 1993.
[42] R. Mosleh, C. Panico, and M. Efendiyev, *Numerical investigation of a diffusive SIR model: Focus on positivity preservation*, Mathematical Methods in the Applied Sciences, (2026).
[43] S. Nüsslein, H. Ranocha, and D. I. Ketcheson, *Positivity-preserving adaptive Runge–Kutta methods*, Communications in Applied Mathematics and Computational Science, 16 (2021), pp. 155–179.
[44] J. R. Ockendon, *Applied partial differential equations*, Oxford University Press, 2003.
[45] N. Özdoğan and B. Arslan, *Nonstandard finite difference theta approaches to the predator–prey system*, Mathematical Methods in the Applied Sciences, (2026).

[46] K. Para, S. Sungnul, S. Sirisubtawee, and S. Phongthanapanich, *A comparison of numerical solutions for advection-diffusion-reaction equations between finite volume and finite difference methods.*, Engineering Letters, 30 (2022).
[47] K. C. Patidar, *Nonstandard finite difference methods: recent trends and further developments*, Journal of Difference Equations and Applications, 22 (2016), pp. 817–849.
[48] A. A. Pishro, S. Zhang, A. L'Hostis, Q. Hu, Y. Liu, Z. Zhang, V. D. Nguyen, Y. Fu, and T. Li, *Partial differential equations and machine learning integration for transit-oriented development*, Applied Soft Computing, (2025), p. 113703.
[49] W. Qin, D. Ding, and X. Ding, *A non-standard finite difference scheme for an advection-diffusion-reaction equation*, Mathematical Methods in the Applied Sciences, 38 (2015), pp. 3308–3321.
[50] G. I. Ramírez-Espinoza and M. Ehrhardt, *Conservative and finite volume methods for the convection-dominated pricing problem*, Advances in Applied Mathematics and Mechanics, 5 (2013), pp. 759–790.
[51] D. S. Ross and A. Cabal, *A QSP PDE model of ADC transport and kinetics in a growing or shrinking tumor*, Journal of Pharmacokinetics and Pharmacodynamics, 52 (2025), p. 57.
[52] W. E. Schiesser, *Mathematical Modeling Approach to Infectious Diseases, A: Cross Diffusion Pde Models for Epidemiology*, World Scientific, 2018.
[53] S. Sharma and G. Samanta, *A Leslie–Gower predator–prey model with disease in prey incorporating a prey refuge*, Chaos, Solitons & Fractals, 70 (2015), pp. 69–84.
[54] R. Shokri Jahandizi, M. Mehdizadeh Khalsaraei, A. Shokri, and A. Khani, *Efficient positivity-preserving NSFD scheme: application to advection-diffusion-reaction equation*, Journal of Applied and Computational Mechanics, 11 (2025), pp. 611–624.
[55] M. J. Simpson, R. J. Murphy, and O. J. Maclaren, *Modelling count data with partial differential equation models in biology*, Journal of Theoretical Biology, 580 (2024), p. 111732.
[56] A. S. Srinivasa Rao, *PDE models in population dynamics*, in Mathematical Demography: Theory and Modeling, Springer, 2025, pp. 19–31.
[57] G. Strang, *On the construction and comparison of difference schemes*, SIAM journal on numerical analysis, 5 (1968), pp. 506–517.
[58] T.-X. Sun, Z.-C. Xue, and H.-T. Zhang, *Spatiotemporal dynamics of a diffusive SI model in the regions of Turing-Hopf bifurcation point*, Nonlinear Dynamics, 113 (2025), pp. 10681–10703.
[59] B. Takács, *An insight on some properties of high order nonstandard linear multistep methods*, Mathematics and Computers in Simulation, (2026).
[60] B. Takács and Y. Hadjimichael, *High order discretization methods for spatial-dependent epidemic models*, Mathematics and Computers in Simulation, 198 (2022), pp. 211–236.
[61] P. Van den Driessche and J. Watmough, *Reproduction numbers and sub-threshold endemic equilibria for compartmental models of disease transmission*, Mathematical biosciences, 180 (2002), pp. 29–48.
[62] A. Viguerie, A. Veneziani, G. Lorenzo, D. Baroli, N. Aretz-Nellesen, A. Patton, T. E. Yankeelov, A. Reali, T. J. Hughes, and F. Auricchio, *Diffusion–reaction compartmental models formulated in a continuum mechanics framework: application to COVID-19, mathematical analysis, and numerical study*, Computational Mechanics, 66 (2020), pp. 1131–1152.
[63] B. Wacker and J. C. Schlüter, *Analysis of a non-standard finite-difference-method for the classical target cell limited dynamical within-host HIV-model-numerics and applications*, Mathematical Biosciences and Engineering, 22 (2025), pp. 2360–2390.
[64] W. Wang and X.-Q. Zhao, *Basic reproduction numbers for reaction-diffusion epidemic models*, SIAM Journal on Applied Dynamical Systems, 11 (2012), pp. 1652–1673.
[65] Y. Wang, M. Zhao, C. Dai, and Y. Deng, *The dynamics of a diffusive nutrient-algae model based upon the Sanyang Wetland*, Mathematical Problems in Engineering, 2015 (2015), p. 251937.
[66] M. W. Yasin, M. Akhtar, M. Alazab, M. Inc, Z. Baber, M. S. Iqbal, and S. Rezapour, *Spatiotemporal dynamics of a reaction-diffusion nutrient-algae model*, Modeling Earth Systems and Environment, 12 (2026), p. 29.
[67] E. Zauderer, *Partial differential equations of applied mathematics*, John Wiley & Sons, 2011.
[68] L. Zhang, *Spatiotemporal patterns in a ratio-dependent food chain model with reaction-diffusion*, Abstract and Applied Analysis, (2014), p. 130851.

Centro de Investigación en Ingeniería Matemática (CI^{2}MA)

PRE-PUBLICACIONES 2026

2026-11 Esteban Henriquez, Manuel Solano: *An unfitted HDG method for a distributed optimal convection-diffusion control problem*

2026-12 Sergio Caucao, Gabriel N. Gatica, Luis F. Gatica, Cristian Inzunza: *A priori and a posteriori error analysis of a mixed FEM for stationary convective Brinkman-Forchheimer flows with variable porosity*

2026-13 Jessika Camaño, Ricardo Oyarzúa, Katherine Rojo, Segundo Villa-Fuentes: *A mixed finite element method based on pseudostress and stream-function for the Navier–Stokes problem in 2D*

2026-14 Raimund Bürger, Cipriano Escalante, Enrique D. Fernández Nieto, Jorge Moya: *A two-dimensional multilayer shallow water model of tsunami-forest interaction*

2026-15 Alonso J. Bustos, Sergio Caucao: *A posteriori error analysis of two mixed formulations for a coupled Brinkman–Forchheimer and convection-diffusion-reaction system*

2026-16 Gabriel N. Gatica, Salim Meddahi, Kevin W. Pucha-Atan, Ricardo Ruiz-Baier: *A Banach spaces-based fully mixed finite element method for the thermo-electro-hydrodynamic Boussinesq problem*

2026-17 Tomás Barrios, Edwin Behrens, Rommel Bustinza, Jose M. Cascon: *A stabilized displacement - stress formulation for a linear elasticity problema with mixed boundary conditions*

2026-18 Gonzalo A. Benavides, Sergio Caucao, Gabriel N. Gatica, Yuri D. Sobral: *New Banach spaces-based mixed finite element methods for steady-state flows of magnetic fluids*

2026-19 Fahim Aslam, Marcelo Cavalcanti, Zayd Hajjej, You Haiyang Lin Bo, Mauricio Sepúlveda: *Blow-up of a Lamé system with fractional damping and infinite memory: theoretical and numerical study*

2026-20 Gabriel N. Gatica, Salim Meddahi: *A hybridizable discontinuous Galerkin method for the elasto–acoustic transmission problem*

2026-21 Idulfo Arrocha, Raimund Bürger, María Gómez, Yolanda Vásquez: *Modeling and numerical simulation of the colonization of plant growth-promoting bacteria in the rice rhizosphere*

2026-22 Abraham J. Arenas, Juan Barajas-Calonge, Gilberto González-Parra, Luis M. Villada: *Convergence analysis of a nonstandard finite volume method for a diffusion-production-destruction model*

Para obtener copias de las Pre-Publicaciones, escribir o llamar a: Director, Centro de Investigación en Ingeniería Matemática, Universidad de Concepción, Casilla 160-C, Concepción, Chile, Tel.: 41-2661324, o bien, visitar la página web del centro: `http://www.ci2ma.udec.cl`



Centro de Investigación en
Ingeniería Matemática (CI²MA)
Universidad de Concepción

Casilla 160-C, Concepción, Chile
Tel.: 56-41-2661324/2661554/2661316
http://www.ci2ma.udec.cl